UNIVERSITY OF NAPLES FEDERICO II

PH.D. PROGRAM IN

CLINICAL AND EXPERIMENTAL MEDICINE

CURRICULUM IN TRANSLATIONAL MEDICAL SCIENCES

XXXVIII Cycle

(Years 2022-2025)

Chairman: Prof. Francesco Beguinot

PH.D. THESIS

ANTITUMORAL EFFECT OF IL-33 AND ITS ROLE AS COMBINATORY AGENT WITH DECITABINE (5-AZA-2'-DEOXYCYTIDINE) AGAINST METASTATIC MELANOMA. A MULTIDISCIPLINARY STUDY INVOLVING IN VITRO, IN VIVO AND "ON CHIP" APPROACHES.

TUTOR

Prof.ssa Gilda Varricchi

PH.D. STUDENT

Dr. Francesco Noto

MATR. N. DR996560

SUPERVISOR

Dr. Fabrizio Mattei

1. INTRODUCTION

1.1 Biology of IL-33

Interleukin-33 (IL-33) is a member of the IL-1 family of cytokines that is constitutively expressed in the nucleus of epithelial, endothelial and fibroblast-like cells. Upon cell stress, damage or necrosis, IL-33 is released into the cytoplasm to exert its primary role as an alarmin by binding to its specific receptor ST2 (Wen Jie Yeoh et al. 2022). Endogenous IL-33 was first visualized as a nuclear protein highly concentrated in high endothelial venules (HEVs), specialized blood vessels that mediate the entry of lymphocytes into lymphoid organs and therefore named "nuclear factor from high endothelial venules" (NF-HEV). (Baekkevold E.S. et al. 2003). IL-33 was categorized into the IL-1 family of cytokines due to structural similarities and to its binding to a heterodimer receptor constituted by IL1RAcP (encoded by IL1RAP) and ST2 (encoded by IL1RL1, and representing the IL-33-specific moiety of the receptor), which belongs to the IL-1 family of receptors (Dinarello C. A. et al. 2018). Like other IL-1 family of cytokines, IL-33 plays a major role in the initiation and amplification of immune responses in inflammatory, infectious and autoimmune diseases after release from cells during necrosis or tissue injury (Scott, I.C. et al., 2018; Cayrol C, Girard JP. et al 2018).

Similar to IL-1β and IL-18, IL-33 is synthesized in a full-length form (270 amino acids in humans and 266 aa in mice) that is found both in the nucleus and outside the cell. The N-terminus (1–75 aa) contains a nuclear localization sequence, a homeodomain-like helix-turn-helix DNA-binding domain and a chromatin-binding domain (Carriere, V. et al. 2007). Intracellular IL-33 can regulate gene expression by different mechanisms. This cytokine binds to the nucleosome acidic patch in histone H2A-H2B dimers into the heterochromatin, where it modulates higher-order chromatin structure and regulates gene expression (Roussel L, et al. 2008.). Serine proteases from neutrophils (cathepsin G, neutrophil elastase and proteinase-3), mast cells (chymase and tryptase), and cytotoxic lymphocytes (granzyme B) can process the N-terminal IL-33 into mature forms with up to 30-fold more potent activity (Scott, I.C. et al., 2018; Lefrancais E. et al. 2012; Lefrançais E. et al. 2014).

As for its receptor, transmembrane form and a soluble form of ST2 (sST2) are generated from a single mRNA through differential expression of two distinct promoters and alternative splicing. IL-33 binding to ST2 leads to IL-1RAcP recruitment and the formation of a heterodimeric signaling complex that involves myeloid differentiation primary response protein

88 (MYD88), IL-1R-associated kinase 1 (IRAK1), IRAK4 and tumor necrosis factor (TNF) receptor-associated factor 6 (TRAF6) and the activation of mitogen-activated protein kinases (MAPKs) and nuclear factor-κB (NF-κB) (Liew, F. et al. 2016).

While IL1RAP is expressed at low levels by all cells, including immune cells, ST2 is expressed primarily by immune cells. Th2-related cells, such as eosinophils, basophils, mast cells, a subset of regulatory T cells (Treg) and type 2 innate lymphoid cells (ILC2), but also by Th1 cells, CD8+ T cells, NK cells, macrophages, neutrophils, dendritic cells (DC) and B cells have all been reported to express ST2 (Afferni et al. 2018, Liew F.Y. et al. 2016). Therefore, IL-33 is capable of stimulating both of Th1 and Th2 type of immune responses playing a role in a variety of pathologies, such as asthma, allergy, cardiovascular diseases, chronic obstructive pulmonary disease (COPD) and cancer (Andreone S. et al. 2020, Liew F.Y. et al. 2016).

1.2 IL-33 and Cancer

IL-33 exhibits pleiotropic functions not only in inflammatory diseases but also in cancer. Emerging evidences have shown that this cytokine may have dual, pro-tumorigenic and anti-tumorigenic function, depending on tumor and cellular context, expression levels, bioactivity and the nature of the microenvironment (Afferni et al. 2018). The involvement of IL-33/ST2 axis in cancer pathogenesis was first reported by Jovanovic and co-workers in 2011 (Jovanovic I. et al. 2011). Using ST2-deficient ($ST2^{-/-}$) mice, these authors demonstrated that the lack of ST2 in female mice suppressed 4T1 breast tumor growth and metastasis. Serum levels of IL-17, interferon (IFN)-γ, and TNF-α were elevated, accompanied by increased intra-tumor accumulation of activated natural killer (NK) cells and CD8+T cells. These results suggested that the loss of IL-33/ST2 signaling could promote Th1/Th17 polarization of the innate and acquired immune responses. (Jovanovic I. et al. 2011). Similarly, the suppression of sST2 reduced the Erb-B2-induced cell motility in breast cancer cells (Gillibert-Duplantier J. et al. 2011).

Similar outcome in understating IL-33/ST2 axis role in cancer have been shown from studies in colorectal cancer (CRC) models. Akimoto and colleagues showed that expression of sST2 was inversely correlated to malignant growth of CRC and was downregulated in highly metastatic cells compared with low metastatic cells. Knockdown of sST2 in low-metastatic cells enhanced tumor growth, metastasis and angiogenesis, while its overexpression in high-metastatic cells suppressed these processes. Overexpression of circulating levels of an sST2-Fc protein fusion exerted suppressive effects, through the reprogramming of the tumor

microenvironment (TME) by suppressing angiogenesis, Th1- and Th2-immune responses, macrophage infiltration and M2a macrophage polarization. These findings underline that sST2 function represent a negative regulator of CRC malignancy by remodeling the TME (Akimoto M. et al. 2016). Recent studies reported that IL-33 is produced by tumor vasculature and malignant cells in human CRC. Administration or overexpression of IL-33 induced tumor sphere formation and protected cells from chemotherapy-induced apoptosis (Larsen KM, 2018). These studies suggest that IL-33/ST2 signaling induced CRC stemness by activating core stem cell genes such as NANOG, NOTCH3, and OCT3/4, and by inducing the phosphorylation of c-Jun N terminal kinase (JNK) to activate c-Jun and enhance its binding to the promoters of these genes. Moreover, in $Apc^{Min/+}$ mice and chemically-induced CRC mouse model, while IL-33 activity was linked with proteases and cytokines related to the development of polyp, genetic ablation of ST2 protected tumor development by reducing the frequency of $ST2^+$ Treg cells in the TME (Pastille E. et al. 2019). In human CRC patients, ST2L protein (the receptor isoform of ST2 mediating intracellular signaling) is decreased in tumor tissues compared to adjacent healthy mucosa, with lower expression along tumor grades suggesting a complex regulatory role for IL-33/ST2 axis in tumorigenesis.

IL-33 is conventionally known to promote Th2 differentiation in naïve $CD4^+$ T cells. However, anti-tumor activity is usually attributed to Th1 cells, supporting recognition and elimination of transformed tumor cells by cytotoxic lymphocytes (Fournié Jean-Jacques et al. 2018). Recent studies implicate that IL-33 may also induce an anti-tumor response by promoting Th1 activity. Specifically, under condition of co-stimulation with IL-12, IL-33 was able to potentiate and promote the early differentiation of $ST2^+$ naïve T cells into Th1 cells *in vitro* (Mousa Komai-Koma, et al 2016). In a human papillomavirus (HPV)-associated mouse tumor model, exogenous IL-33 administrations enhanced IFN-γ and TNFα secretion by $CD4^+$ T cells, leading to the upregulation of antigen-specific IgG and subsequent tumor regression (Villarreal D.O. et al. 2014). Similarly, endogenous IL-33 was reported to enhance expression of IFN-γ^+ in $CD4^+$ T cells in murine models of CRC (Xia Yulong et al. 2019). An interesting study conducted by Amisaki and colleagues evidenced the antitumoral effect of IL-33 in pancreatic ductal carcinoma (PDAC) by activating ILC2, which induce the formation of tertiary lymphoid structures (TLS) within the tumor. These structures function as an ectopic organ promoting local robust immune response against the tumor. IL-33 is released from damaged or inflamed tissues and activate the ILC2 inducing them the expression of lymphotoxin (LT) that engages on LT receptors on intertumoral myeloid cells. Specifically, the administration of recombinant IL-33 further increased intertumoral TLS, expanded

KLRG1+ ILC2, and slowed tumor growth in a dose-dependent manner, demonstrating that the IL-33–ILC2–TLS axis robustly enhances antitumor immunity in PDAC (Amikasi et al. 2025).

Several lines of evidence indicate that in melanoma IL-33 exerts antitumoral activities through the stimulation of various immune cells (Afferni et al. 2018; Andreone et al. 2020). Early studies showed that transgenic host (Xiao P. et al. 2015) and tumoral (Gao X et al. 2015) expression of IL-33 inhibits tumor growth and metastasis in B16 melanoma mouse models by stimulating NK and CD8+ T cell responses. Dominguez and colleagues reported that IL-33 treatment both expanded CD8+ T cell-producing IFN-γ and stimulated DC antigen cross-presentation in transplantable and BRAFV600EPTEN-inducible melanoma models (Dominguez D. et al. 2017). Another study showed that in mice transplanted with B16 melanoma cells engineered to secrete IL-33 a high number of intratumoral ILC2 with potent antitumor activity is established. In this model, local production of IL-33 promoted a TME characterized by dysfunctional angiogenesis/hypoxia/reactive oxygen species axis supporting ILC2-induced apoptosis (Lucarini V. et al. 2017). Our group demonstrated that IL-33 inhibits melanoma tumor growth and pulmonary metastasis in mice in an eosinophil-dependent manner. We observed increased metastatic load and reduced lung eosinophilia in ST2−/− compared to wild type (WT) mice. Moreover, *in vivo* depletion of eosinophils completely abolished the anti-tumor and anti-metastatic effects of IL-33 (Lucarini V. et al. 2017). We further showed that eosinophils activated with IL-33 exhibit an enhanced CD11b/CD18-mediated binding to tumor cells and concentrated their lytic granules to the immune synapsis leading to a highly efficient, contact-dependent degranulation and tumor cell killing (Andreone et al. 2019). Recently, we reported that mouse and human eosinophils stimulated with IL-33 increase their release of extracellular vesicles (EVs) enriched with tumor suppressor mRNAs and proteins. These EVs are efficiently incorporated by tumor cells, causing transcriptional reprogramming that induces cell cycle arrest, upregulates epithelial markers such as E-cadherin, downregulates mesenchymal markers, and blocks epithelial-to-mesenchymal transition (EMT). Functionally, tumor cells treated with IL-33-activated eosinophil EVs display reduced proliferation, invasion, and metastatic potential in murine models and human melanoma spheroid cultures (Gambardella A.R. et al. 2024).

In conclusion, these findings suggest a context-dependent, often tumor suppressive role for IL-33 in selected cancer types, and that in melanoma this cytokine can exert an efficient antitumoral effect by reshaping the TME and by stimulating several immune effector cells. Of note, IL-33 has been found to be both required for immune checkpoint blockade

efficacy (Chen L. et al. 2020 Blomberg O.S. et al. 2022) and to improve the therapeutic response to immune checkpoint inhibitors (ICI), such as PD-1, in tumor-bearing mice (Blomberg O.S. et al. 2023; Hollande C. et al. 2019, Moral J.A. et al. 2015), thus providing rationale for combination therapies.

1.3 Melanoma

Melanoma originates from the malignant transformation of melanocytes that have undergone multiple genetic and epigenetic modifications. In melanoma, the Ras-Raf-MEK-ERK (MAPK) signaling pathway is constitutively activated through multiple mechanisms. Mutations of *B-RAF* have been proposed to contribute to melanoma development. V600E accounts for >60% of *B-RAF* mutations in melanoma and causes a substantial increase in BRAF kinase activity (Russo AE. et al .2009). It has been suggested that *BRAF* mutations in melanocytic lesions arise from DNA damage induced by UV radiation (Candido S. et al. 2014). Despite the importance of BRAF V600E mutation, epigenetic modifications are important in the alterations for melanoma progression. Epigenetic dysregulation that modifies the activity of tumor suppressor genes involved in cell cycle, growth and proliferation like CDKN2A, MTAP, PTEN and P53 contribute to melanoma progression and invasion (Raza Zaidi M. et al. 2008, Hunter Shai A. et al. 2015).The CDKN2A is a melanoma susceptibly gene mutated in 20-50% of the familial melanoma cases and the 2-3% of the sporadic melanoma (Kostaki, M. et al. 2014). Its alteration consists primarily in the hypermethylation of its promoters. Aberrant methylation of this locus provides an advantage for melanoma growth and metastatization, highlighting the role of epigenetic alteration during melanoma progression. Additional oncogenes that can be regulated by epigenetic alterations include RAS (Yi S.-J., 2018), ERK, MITF (Lahtz C. et al. 2010;), c-jun and BLC-2 (Leiter U. et al. 2000). PTEN (phosphatase and tensin homolog) is a phosphatase that converts PIP3 (phosphatidylinositol (3,4,5)-phosphate) to PIP2 (phosphatidylinositol 4,5-bisphosphate), suppressing the PI3K/Akt signaling is frequently mutated across different types of cancer, including melanoma, with a reported rate in melanoma cell lines of 30–50% and 5–20% in primary samples. Of note, the hypermethylation of this gene was associated with poor patient prognosis (Lahtz C. et al. 2010;). Moreover, MITF (microphthalmia-associated transcription factor) is very important in melanoma progression as it controls the melanocytes specific proliferation and it is under the control of the BRAFV600E mutation. It works as transcription factor and requires the cromatin-remodeling complex of SWI/SBF to activate melanocyte specific genes (Shaffer S.M., et al. 2017). The methylation patterns of the MITF

promoter can change during the melanoma progression and can be reactivated by hypomethylation (Lauss M. et al 2015).

In conclusion, melanogenesis relies on a multifactor series of mutations and epigenetic dysregulation, mainly involving DNA methylation and chromatin remodeling (Gracia Hernandez M. et al. 2021, Giunta EF. et al. 2021). These epigenetic changes are not only implied in cancer initiation and progress but also in drug resistance, such as to MAPK and ICI, thus becoming attractive targets for testing epigenetic drugs against melanoma.

1.4 DNA Hypomethylating agents and their use in cancer

One of the most widely studied epigenetic modifications in cancer is the aberrant DNA methylation. This could occur both through global DNA hypomethylation, leading to genomic instability and possibly increasing the frequency of mutations and chromosomal abnormalities, and through the hypermethylation of specific genes leading to the impairment of the corresponding protein expression, mainly catalyzed by DNA methyltransferase (DNMT) enzymes (Fazio C. et al. 2018). The plasticity of epigenetic phenomena suggested the feasibility of their targeting by epigenetic drugs, such as DNA hypomethylating agents that can restore the physiologic epigenetic pattern by targeting DNMT enzymes. Among these, the best characterized are DNMT inhibitors (DNMTi) that lead to passive demethylation of genomic DNA following DNA replication. The most widely used DNMTi comprise 5-azacytidine (Vidaza; Baxter Oncology GmbH/Celgene), 5-aza-2′-deoxycytidine [5-aza-CdR, Decitabine, Dacogen (Otsuka America), DrugBank Id: DB01262], zebularine, and RG108 (Maio M. et al 2015). DNMTi have proven effective in inducing/upregulating tumor suppressor gene-expression *in vitro* and *in vivo*, apparently displaying a preferential activity on transformed versus normal cells (Gracia Hernandez M. et al 2021). First generation DNMTi, azacytidine (AZA) and decitabine (DAC), have been FDA approved for the treatment of myelodysplastic syndromes and acute myeloid leukemia (Cataldo, V. D. et al. 2009). DNMTi can potentiate immune recognition through the up-regulation of class I and co-stimulatory molecules, the promotion of CD8 T-cell responses, and the regulation of immune checkpoint molecules (Han J. et al. 2020, Fazio C. et al. 2018). Based on these properties, these epigenetic drugs have become an eligible combinatory therapy to support immunotherapy and overcome cancer resistance.

1.*5 Decitabine: anti-tumor properties and therapeutical potential*

DAC is a 2'-deoxycytidine analog that typically functions by activating methylated and silenced genes by promoter demethylation. This epigenetic drug is phosphorylated intracellularly and incorporated into DNA where it exerts numerous effects on gene expression. DAC has a dual mechanism of action: reactivation of silenced genes (at low drug doses), and cytotoxicity effects (at high drug doses) (Jabbour E. et al 2008). DAC is considered a prodrug, as it requires to be transported into cells and subsequent phosphorylation by distinct kinases to generate the active molecule 5-aza-2'-deoxycytidine-triphosphate, which is incorporated by DNA polymerase during DNA replication (Daskalakis M, et al. 2010). Once incorporated into DNA, DAC is recognized as a substrate by DNMTs, specifically DNMT1. However, the presence of a nitrogen atom at the 5-position (N5 instead of C5) traps the enzyme on the DNA through the irreversible formation of a covalent adduct. (Patel K, et al. 2010)

In melanoma, DAC was reported to cooperate with IL-12 (Stahl M, et al 2019) and ICAM-1 antibody drug conjugates (Zhang P, et al. 2024) Zhang and colleagues discovered that combination of DAC with ICAM-1 antibody-drug conjugates (ADC) enhance antitumor efficacy in melanoma by upregulating ICAM-1 expression and improving ADC internalization by tumor cells. This synergy also increased the immune infiltration with recruitment of CD8 T cells, NK and M1-polarized macrophages and a stronger apoptotic response, highlighting the potential of this combined therapy in preclinical studies. Specifically, DAC upregulates ICAM-1 surface expression activating the cGAS-STING pathway leading to increase of NFkB, JNK and MAPK signaling, therefore making the tumor cells more susceptible to ADC effect (Zhang P. et al 2024).

Combination of DAC and type I IFN (IFN-I) enhances the therapeutic benefit of DNA vaccines in melanoma-bearing mice (Gordy JT et al. 2022, Gordy JT et al. 2020) suggesting that combinatorial regimen of DAC with immunostimulating cytokines is a promising strategy for ameliorating anti-tumor response. Our group showed that DAC increases melanoma susceptibility to the antitumoral effect of IFN-I. Indeed, DAC plus IFN-I promote cell death and reduce proliferation and migration of mouse and human melanoma cells *in vitro*. The combined treatment restricts melanoma growth *in vivo* by altering the immune microenvironment with an increase of tumor cell expression of PD-L1 and tumor-infiltrating CD8 T cells (Lucarini V. et al. 2017). In another study, Xiang and co-workers demonstrated in

a colon cancer and leukemia cancer mice models the ability of DAC to enhance the proliferation on effector CD8 progenitor exhausted T cells (T_{ex}) when combined with anti-PD-1 treatment and improve the cytotoxic effect of T_{ex} compared to the anti-PD-1 alone (Li X. et al. 2023).

Overall, these studies provide a valid rationale for employing DAC as a good coadjuvant agent to overcome the resistance to ICI.

1.6 Melanoma immunotherapy: immune checkpoint inhibitors and combination with anti-cancer agents

Immunotherapy has revolutionized the approach of therapeutic strategies against cancer, particularly melanoma. Unlike conventional anti-cancer agents that directly destroy cancer cells, immunotherapy aims at boosting the immune system's natural ability to fight cancer. Four major groups of immunotherapeutic agents can be described: 1) soluble mediators that act as immune stimulators, such as interferons and granulocyte-monocyte colony-stimulating factor; 2) cancer vaccines based on peptides, whole proteins, viruses, or DNA, or antigen-loaded DC; 3) adoptive cell therapy factors, which consists in the use of the so-called lymphokine activated killer (LAK) cells, tumor-infiltrating lymphocytes (TIL), or CAR cells (Sukari A. et al. 2019); 4) monoclonal antibodies, such as those targeting cancer cells or those that block immune system checkpoints (i.e., ICI).

The identification of immune checkpoint proteins, such as cytotoxic T lymphocyte-associated antigen 4 (CTLA-4), programmed cell death protein 1 (PD-1), and PD-1 ligand 1 (PD-L1), has facilitated the development of monoclonal antibody (mAb)-based drugs that inhibit their activation. These checkpoints regulate the innate and adaptive immune systems, influencing their functionality. Tumors exploit these inhibitory checkpoints to evade immune eradication. In the last few years, the use of anti-PD-1 (pembrolizumab and nivolumab) and anti-CTLA-4 (ipilimumab) has represented a breakthrough for the treatment of malignant melanoma and other aggressive cancers (Ralli M. et al. 2020, Sukari A. et al. 2019, Choubey D et al. 2019, Bomar L. et al. 2019, Coventry BJ. et al. 2019). Pre-requisite of tumor response to ICI is the co-expression by cancer cells of immunogenic tumor antigens and targetable immune checkpoint molecules. The combination of PD-1 and CTLA-4 blockade determined an improved overall survival rate of 58% in clinical trial compared to ipilimumab alone. However, while blockade of CTLA-4 and PD-1 have demonstrated remarkably durable clinical responses, it remains effective only in a subset of patients. Moreover, the primary and acquired resistance

to ICI affects more than a half of patients receiving these agents in the first-line setting (Ottaviano M. et al. 2019).

To address these limitations, new combined treatment strategies are being investigated to overcome immunotherapy resistance, including the use of epigenetic drugs for their ability to act on both immune and tumor cells. In a study conducted by Amaro and co-workers, the second generation DNMTi Guadecitabine was employed in combination with anti-PD-1 and anti-CLTA-4 in a mouse melanoma model. The study demonstrated that the epigenetic drug sensitized the tumor to ICIs and remodeled the immune infiltrate of the TME. They also showed that Guadecitabine improved the expansion and cytotoxic activity of CD8T cells and NK. Simultaneously, this treatment reduced the immunosuppressive cells types including regulatory T cells and myeloid derived suppressor cells. Additionally, Amaro & co-Workers found increased serum level of IFNγ and IFN-induced chemokines such as CXCL9 and CXL10 (Amaro A. et al. 2023).

These interesting findings suggest that combinatory strategies employing ICI and epigenetic modifier drugs can effectively cooperate in the shaping of the immune infiltrate in the TME and therefore overcome the resistance to immunotherapy.

1.7 Microphysiological Systems

The intricate composition of a TME poses a significant barrier to effective cancer immunotherapy, requiring innovative strategies to model and address its challenges. Traditional models, such as 2D cultures, often fail to capture the TME's dynamic, multicellular, and spatially complex nature, limiting their predictive power for therapeutic outcomes. In parallel, animal studies often do not reflect the exact human TME scenarios. To overcome these limitations, innovative microphysiological systems (MPS) that enhance the understanding of tumor-immune interactions and pave the way for more effective immunotherapeutic strategies (Moresi F. et al. 2025).

Although animal models remain useful, their ability to predict human-specific responses is limited by interspecies variations. The precise control of the microenvironment, the real-time cell-cell interactions, the mimicry of human physiology, and the variety of available analyses are all advantages of MPS and organ-on-chip (OoC) that influence the effectiveness of the preclinical model and the discovery of new therapeutic strategies. These technologies have been employed in various fields of research, including cancer immunology, facilitating drug development processes (Lam M. et al. 2021; Mattei F. et al. 2021). In this context, MPS provide

key platforms for investigating immune-cancer cells crosstalk exploiting the multifunctional application in the analysis of the intricate structure of the tumor immune microenvironment (TiME). For example, in a study by Nguyen and colleagues, an OoC approach was used to analyze NK cell phenotype and function in the context of colorectal adenocarcinoma. They included functional cardiac tissue to investigate tolerability and demonstrated selective NK cell-mediated tumor cell killing with varying responses. This was achieved with no structural defects but a decreased beating frequency of the cardiac tissue. Such a model exemplifies how tolerability can be evaluated in microfluidic tumor models alongside efficacy (Nguyen O.T.P et al. 2021). In another study, Jenkins and co-workers evaluated ex vivo responses to ICI using murine and patient-derived organotypic tumor spheroids (MDOTS/PDOTS). These MDOTS/PDOTS, isolated from mouse and human tumors, retain autologous lymphoid and myeloid cell populations and respond to ICB in short-term 3D microfluidic culture. MDOTS profiling demonstrated that TBK1/IKKε inhibition enhanced the response to PD-1 blockade, effectively predicting tumor response *in vivo*. Systematic profiling of secreted cytokines in PDOTS captured key features associated with response and resistance to PD-1 blockade. (Russell W. Jenkins et al. 2018)

Previous studies from our group used microfluidic assays to investigate the requirement of specific immune cell-expressed molecules for the crosstalk with cancer cells. Immune-deficient interferon regulatory factor-8 (IRF-$8^{-/-}$) mice develop larger melanoma tumors with less immune cell infiltration than WT animals. Microfluidic chip experiments demonstrated that immune spleen cells lacking IRF-8 do not migrate toward melanoma cells nor interact with them as efficiently as WT immune cells, suggesting a mechanism to explain the defective immune surveillance and tumor growth control in IRF-$8^{-/-}$ melanoma-bearing mice (Businaro L. et al 2013). In a similar study, the therapeutic effects of anthracyclines were abrogated in tumor-bearing formyl peptide receptor 1 (Fpr1) knockout mice due to impaired antitumor immunity. Experiments performed in a microfluidic chip demonstrated the requirement of immune cell-expressed Fpr1 for engaging in stable interactions between mouse and human dying cancer cells and immune cells (Vacchelli et al. 2015). More recently, microfluidic chips have been employed to compare single or combined anti-cancer agents for their ability to elicit immune cell migration in a competitive fashion. These microfluidic competitive assays allowed to demonstrate the superior ability of combined DAC plus IFN-I treatment, with respect to single agents, to stimulate immune cell recruitment towards melanoma cells both in murine and human settings (Lucarini V. et al. 2017).

MPS, particularly OoC technologies, have revolutionized cancer research by offering more physiologically relevant models for studying tumor biology and treatment efficacy. These platforms enable highly controlled cellular microenvironments and real-time visualization of cell-cell interactions, crucial for understanding cancer cell behavior and evaluating therapeutic interventions.

2. AIM OF THE STUDY

The treatment of metastatic melanoma is still a challenge in clinical oncology (Switzer et al. 2022). Immunotherapy and "targeted" therapies against tumor antigens have proven notable efficacy but on a limited number of patients. Immunotherapy with ICI limits tumor immune escape yet only for approximately a third of patients and in most cases for a limited time. Several approaches to overcome resistance to ICI are being investigated among which the addition of epigenetic drugs that are expected to act on both immune and tumor cells (Amaro A. et al. 2023).

In melanoma, aberrant DNA hypermethylation is frequently observed, resulting in the silencing of several genes involved in cell cycle regulation, apoptosis, tumor growth and drug resistance. The use of DNMTi holds promise for melanoma treatment due to their ability to promote immune recognition by re-activating silenced genes. Combination of DAC with immunostimulatory cytokines, such as IFN-I, is highly effective in contrasting the growth of mouse and human melanoma *in vitro* and *in vivo* through direct effects and by remodeling the tumor-immune microenvironment (Lucarini V. et al, 2017). Both intratumoral expression and exogenous administration of IL-33 promote anti-tumor responses by recruiting or activating eosinophils, dendritic cells ILC2 NK and CD8+ T cells (Andreone S. et al 2020, Andreone S. et al 2019, Dominguez D. et al. 2017, Gao X, et al. 2015, Kim J et al. 2016). In the TME, tumor cells and stromal cells such as fibroblast, epithelial cells and infiltrating immune cells are critical sources of IL-33. Expression of IL-33 by tumor cells stimulates CD8 T cell-mediated anti-tumor activity in various cancer models, including colorectal cancer (Yeoh WJ. et al. 2022), pancreatic ductal adenocarcinoma, melanoma and breast cancer (Dixit A. et al. 2022), and is required for ICI efficacy (Blomberg OS et al. 2023 Chen L .et al. 2020).

The aim of this study was to investigate the synergistic potential of DAC combined to IL-33/ST2 axis against melanoma. Specifically, we explored how the combinatory action reshapes the TME and enhances response to PD1 blockade in melanoma-bearing mice. We further investigated the mechanism by which DAC epigenetically induces IL-33 expression and

that the IL-33/ST2 pathway drives immune migratory responses. To achieve these objectives, we employed *in vitro*, *in vivo* and OoC systems. In spheroids of mouse and human melanoma cells, we investigated the direct anti-tumor activities of DAC alone or combined with IL-33. *In vivo*, we explored the benefits of DAC/IL-33 combination in contrasting tumor growth in mice transplanted with B16.F10 melanoma cells. We dissected how the combined DAC/IL-33 treatment affected the immune recruitment (i.e., T cells and eosinophils) at the tumor site, PD-1 expression, and its potential to ameliorate the therapeutic response to PD-1 blockade *in vivo*. We further evaluated the requirement of endogenous DAC/IL-33 axis for DAC *in vivo* therapeutic response and cancer-immune crosstalk by employing ST2-deficient ($ST2^{-/-}$) mice. In a microfluidic-based dual-TME competitive migration assay, we assessed the chemotactic response generated by DAC/IL-33 to spleen cells from naïve WT and $ST2^{-/-}$ mice, as well as in human PBMCs. We also conducted methylation studies to explore epigenetic control of IL-33 expression by DAC in mouse and human melanoma cells. Finally, to improve the translational potential of this project, we used Organix™, an advanced microfluidics device to study vascularized melanoma spheroids within a 3D TME (Adriani G. et al. 2024). These experimental settings allowed us to analyze the effect of this combinatory therapy in a more complex but still reproducible human model. Through confocal imaging, flow cytometry and RT-qPCR analyses, we confirmed more accurately the effect of DAC/IL-33 combination in the recruitment of immune cells within the TME. The results of our studies could provide new knowledge useful for the development of therapeutic strategies based on the combination of epigenetic and immunotherapeutic drugs with higher efficiency for melanoma patients.

3. METHODS

3.1 Cell lines and chemical reagents

Murine B16.F10 melanoma cells were purchased from the American Type Cell Collection (ATCC, Manassas, VA, USA; CRL-6475). Human A375M melanoma cells (CVCL_B222) were provided by Dr. Alessandra Carè (Istituto Superiore di Sanità, Rome, Italy). Human and mouse melanoma cells were cultured in Dulbecco's Modified Eagle's Medium (DMEM) supplemented with 10% of Fetal Bovine Serum (FBS) 1% glutamine, 1% antibiotic-antimycotic (all purchased from Euroclone, Pero, MI, Italy). Normal human lung fibroblasts (NHLF) (Lonza, Basel, Switzerland) were cultured in complete DMEM. GFP-tagged human umbilical

vein endothelial cells (HUVEC) (Lonza) were cultured in EGM-2 medium supplemented with 5 % heat-inactivated FBS and 1 % penicillin/streptomycin.

Cell lines were routinely tested for morphology, absence of mycoplasma and passaged for no more than 4 times from thawing. Chemical reagents included Decitabine (A3656 5-Aza-2'-deoxycytidine; DAC) cisplatin (C2210000; CDDP) and doxorubicin hydrochloride (D1515; DOXO) and were purchased from Sigma Aldrich (Saint Louis, MO, USA). Recombinant mouse IL-33 (rmIL-33) carrier-free (amino acids Ser109-Ile266) was purchased from Biolegend (San Diego, CA, USA). Recombinant human IL-33 (rhIL-33) was purchased from Cell Guidance Systems (Cambridge, UK).

3.2 MTS Assay

One thousand B16.F10 and A375M melanoma cells were seeded in 200 µL of fresh medium in flat 96-well plates (Corning) in the absence or presence of graded concentrations of DAC, IL-33 (100 ng/mL) or their combination. After 24 h, 48 h and 72 h of culture, 20 µL of 3-(4,5-dimethylthiazol-2-yl)-5- (3-carboxymethoxyphenyl)-2-(4-sulfophenyl)-2H-tetrazolium (MTS; CellTiter 96™ AQ_{ueous} Nonradioactive Cell Proliferation Assay Kit, Promega, Madison, WI, USA) were added to each well and cells further incubated for 1 hour at 37°C in 5% CO_2. Absorbance was measured in a spectrophotometer at a wavelength of 490 nm.

3.3 Tumor spheroid assay

Tumor spheroids were established from murine B16.F10 and human A375M melanoma cells and seeded in ultralow attachment surface (uLAs) 96 well plates (Corning, NY, USA). Five hundred cells were cultured in 100 µL of complete DMEM. B16.F10 cells were treated with 0.1 µM DAC, 100 ng/mL rmIL-33, alone or in combination. A375M cells were treated with 0.25 µM DAC 100 ng/mL rhIL-33, alone or in combination. Each experimental condition was tested in five replicates. Visible channel microphotographs were captured at different time of culture by using an EVOS-FL microscope (Life Technologies, Carlsbad, CA, USA). Up to four regions were acquired per each spheroid well. Images were then subjected to particle analysis quantification by using the homonym ImageJ plugin (https://imagej.net/ij/). An optimal thresholding algorithm was chosen for each region, depending on visible light dispersion and distribution. Spheroid area was calculated and used as representative morphometric parameter.

3.4 Mice and in vivo treatments

C57BL/6J mice (Envigo, San Pietro al Natisone, UD, Italy) and $ST2^{-/-}$ mice on a C57BL/6J background (kindly provided by Dr. Andrew N. McKenzie) were housed in the animal facility at the Istituto Superiore di Sanità (Rome, Italy). To assess the evaluation of the combined DAC/IL-33 effect on melanoma growth, C57Bl/6 mice were injected subcutaneously with 0.8 x 10^6 B16.F10 cells. Mice were then injected once intraperitoneal (i.p.) with DAC (1 mg/kg,) and/or intratumoral (i.t.) with rmIL-33 (0.4 μg per mouse), when the tumor reached 3 mm of diameter (approximately 6-7 days post-transplant). IL-33 injections were repeated for 4 consecutive days for a total of five administrations. To study the PD-1 blockade effect, melanoma-bearing mice treated with DAC plus IL-33 received three i.p. injections of 250 μg/mouse PD-1 mAb (clone 29F.1A12, Leinco Technologies, Saint Louis, MO, USA), every three days starting from the last day of IL-33 administration. Control groups included mice receiving IL-33 alone, DAC alone, PD-1 mAb alone, IL-33 plus PD-1 mAb, or DAC plus PD-1 mAb. For the evaluation of chemo-drug response, C57BL/6J wild-type and $ST2^{-/-}$ melanoma-bearing mice received a single injection of DAC (1 mg/kg, i.p.), CDDP (2.5 mg/kg i.t.) or DOXO (2 mM i.t.). Tumor size and growth in all mice was measured twice a week by caliper. Where indicated, mice were sacrificed at appropriate times for *ex vivo* analyses.

3.5 Flow cytometry analysis of tumor-infiltrating immune cells

For flow cytometry analysis, melanoma explants were cut into small fragments using curved scissors and then digested in a medium containing type III collagenase (1 mg/ml; Worthington Biochemicals, Lakewood, NJ, USA) and DNase I (325 KU/mL; Sigma) for 30 min at room temperature in agitation, followed by EDTA (0.1 M pH 7.2) for additional 5 minutes. The homogenate was then passed through a cell strainer, and the resulting suspension was treated with Ammonium-Chloride-Potassium (ACK) lysis buffer (8.26 g NH_4Cl, 1g $KHCO_3$, 0.037g EDTA 0,1M in 1 L of distillated sterile H_2O) to eliminate erythrocytes. Cells were incubated with LIVE/DEAD® Fixable Near-IR Dead Cells Stain Kit (Life technologies) and then labelled with fluorescent antibodies (mAbs). We used these following mAbs: anti-CD45 (clone 30-F11) and anti-Siglec-F (clone E50-2440) from BD Bioscience (Franklin Lakes, NJ, USA); anti-CD3 (clone 145-2C11), anti-CD4 (clone GK1.5), anti-CD8 (clone 53-6.7), anti-CD11b (clone M1/70), anti Ly6G (clone 1A8), all from Biolegend; anti-CD279 (PD-1; clone J43) from eBioscience (San Diego, CA, USA). Biotinylated antibodies were detected by Streptavidin PercP-Cy5.5 or eFluor450 (eBioscience). Samples were run on a Gallios flow cytometer and

analyzed with the Kaluza Analysis Software (Beckman Coulter). Cell populations were defined as follows: $CD45^+CD3^+$ $CD11b^-CD4^+CD8^-$ (CD4 T cells); $CD45^+CD3^+CD11b^-CD4^-CD8^+$ (CD8 T cells); $CD45^+CD11b^{hi}SiglecF^{hi}Ly6G^-$ (eosinophils); $CD45^+CD11b^{hi}SiglecF^-Ly6G^+$ (G-MDSC).

3.6 Quantitative reverse transcription-PCR (qPCR)

Total RNA from tumor tissues was isolated by using Trisure reagent (cat n° BIO-38033, Meridian Bioscience, Memphis, TN, US) and reverse transcription of the messenger RNA (mRNA) was carried out with the Tetro cDNA Synthesis kit (BIO.65043, Meridian Bioscience). Quantitative reverse transcription-PCR (qPCR) was performed using SensiFAST SYBR Lo-ROX Kit containing the fluorescent dye SYBR Green (BIO-94020, Meridian Bioscience). Forward and reverse primers sequences (listed in the Table 1) were purchased from Eurofins Genomics (Louisville, KY, USA) and from Integreted DNA Technologies (IDT, Singapore, Singapore) (listed in Table 2). The conditions of the real-time PCR reaction were: 15 sec at 95°C, 30 second at 60°C and 45 seconds at 72°C for 45 cycles using the Applied Biosystem™ 7500 Fast Real-Time PCR System apparatus. Specificity and quality of amplicons in each sample were detected with by dissociation curves elaborated by the applicative software of the machine (7500 Software, version 2.0.6). Triplicates were performed for each experimental point. For quantization, threshold cycle (CT) values were determined by the Sequence Detection System software (Applied Biosystems, Waltham, MA, US), and data were presented as fold expression vs. HPRT housekeeping gene (2-ΔCt method).

Table 1. Primer pairs used for RT-qPCR.

Human	
Gene	**Primer sequence (Forward/Reverse, 5' --> 3')**
IL33	AATCAGGTGACGGTGTTG
	ACACTCCAGGATCAGTCTTG
HPRT	TGACACTGGCAAAACAATGCA
	GGTCCTTTTCACCAGCAAGCT
Mouse	
Gene	**Primer sequence (Forward/Reverse, 5' --> 3')**
Il33	Biorad #10025636
Lag3	TGTCTACAACTCACCGCGTC
	CTCCAGACCCAGAACCTTGA
Tim3	TTGGAGTGGGAGTCTCCTGCT

	ATCCTGACTGCTCCTGCATT
Gzmb	GATCGGGAGTGTGAGTCCTAC
	GAAAGCACGTGGAGGTGAAC
Pd1	GATGCCCGCTTCCAGATCAT
	AGGTCTCCAGGATTCTCTCTGTTA
Tigit	AAGCTCAGTGGCTCAGTTCC
	TCAGGTTCCATTCCTGTGGC
Cxcl10	CTCTCGCAAGGACGGTCCGC
	TCCGGATTCAGACATCTCTGCTCAT
Cxcl9	GGAGTTCGAGGAACCCTAGTGA
	GTTCTTCAGTGTAGCAATGATTTCAG
Ccl5	ATATGGCTCGGACACCACTC
	GTGACAAACACGACTGCAAGA
Perforin	GTGTCGCATGTACAGTTTTCG
	TGTGGTAAGCATGCTCTGTG
Tnfα	CATCTTCTCAAAATTCGAGTGACAA
	TGGGAGTAGACAAGGTACAACCC
Ifnγ	TCAAGTGGCATAGATGTGGAAGAA
	TGGCTCTGCAGGATTTTCATG
Ccl11	CCCCAAGAAGAAGTGGGTCC
	GGGCGACTGGTGCTGATATT
St2	GAATGGGACTTTGGGCTTTG
	CAGGACGATTTACTGCCCTCC
Il12p40	GGAAGCACGGCAGCAGAATA
	AACTTGAGGGAGAAGTAGGAATGG
Hprt	CTGGTGAAAAGGACCTCTCG
	TGAAGTACTCATTATAGTCAAGGGCA

Table 2. Primer pairs used for RT-qPCR purchased from IDT.

Human	
Gene	**Primer sequence (Forward/Reverse, 5' --> 3')**
V-CAM	GGGAAGATGGTCGTGATCCTT
	TCTGGGGTGGTCTCGATTTTA
GADPH	ACCACAGTCCATGCCATCAC
	TCACCACCCTGTTGCTGTA

3.7 Isolation of mouse spleen cells and human peripheral blood mononuclear cells (PBMCs)

Spleens were removed from naïve C57Bl/6J wild-type or ST2$^{-/-}$ mice were mechanically dissociated through a cell strainer with the plunger of a syringe . The resulting cell suspension was treated with ACK lysis buffer to eliminate red blood cells. Peripheral blood mononuclear

cells (PBMCs) were obtained from healthy donor buffy coats by Ficoll-Hypaque density-gradient centrifugation by using Lymphosep, Lymphocyte Separation Media (L0560, Biowest, Nuaillé, France).

3.8 Competitive migration assay in 3D microfluidic chips

Microfluidic chips for co-culture competitive assay were fabricated in polydimethylsiloxane (PDMS). The devices consist of two center end closed channels adjacent to two cell culture compartments. The two main culture channels and the center channel were connected by micro-sized channels. Melanoma cells (B16.F10 cells or A375M cells) were labeled with the membrane dye PKH67 Green Fluorescence Cell Linker (MINI67, Sigma Aldrich) and then resuspended in ice cold Matrigel (2 mg/ml; Corning). Where indicated, DAC and IL-33 were added single or combined to the melanoma cell-Matrigel mixture. For mouse cells, DAC was used at 0.1 μM and rmIL-33 at 100 ng/ml. For human cells, DAC was used at 0.25 μM and rhIL-33 at 100 ng/ml. The melanoma cell-Matrigel mixtures (2 x 10^4 cells in 5 μl) were loaded in the two narrow lateral chambers and the devices were placed at 37 °C for 30 minutes to allow gel solidification. In a second step, immune cells (mouse spleen cells or human PBMC) were labelled with PKH26 Red Fluorescence Cell Linker (MINI26, Sigma Aldrich), resuspended in RPMI complete medium and loaded (1 x 10^6 cells in 100 μl) in the central chamber of the device. As a final step, the reservoirs of the lateral chambers were filled with medium and the devices were placed in a 37°C, 5%CO_2 incubator for 48 h. Phase contrast, visible and fluorescence photomicrographs were generated by using EVOS-FL fluorescence microscope (Life Technologies) provided with built-in imaging software for imaging overlays. Quantitative fluorescence analysis was carried out with ImageJ software (https://imagej.net/ij/).

3.9 Detection of CD8 T cells in 3D microfluidic chips by fluorescence analysis

PKH26 Red-labelled PBMCs were loaded in the chip together with Matrigel-embedded unlabeled A375M cells exposed to the various treatments in a competitive setting, as described above. After 48 h co-culture, the medium was aspirated from the lateral and central fluidic chambers, and channels were washed with PBS followed by 1% bovine serum albumin (BSA) in PBS. After the washes, staining was carried out with anti-human CD8 Alexa Fluor 488 (clone OKT8; eBioscience) and anti-human CD3 biotin (clone OKT3; Biolegend) followed by Streptavidin Alexa Fluor 647 (eBioscience) for 45 min at 4°C. The devices were fixed with a 2% paraformaldehyde (PFA) and 1% glutaraldehyde solution for 20 min and finally stained

with DAPI (4',6-Diamidino-2-Phenylindole, Dihydrochloride; Invitrogen, Waltham, MA, USA) for 45 min at 4°C for nuclei labelling. Detection of $CD3^+CD8^+$ T cells and their spatial interaction with A375M cells in the Matrigel chambers were performed by laser scanning confocal microscopy (LSCM). The Z-Stack/XY planes 3D images were acquired on a LSCM station Zeiss LSM 900 (Carl Zeiss GmbH, Jena, Germany) in Airyscan mode. Excitation light was obtained by using diode lasers 405 nm, 488 nm, 647 nm and 555 nm. Images and Z-stack/XY planes were obtained and processed by the Zen Blue (v3.2) software (Carl Zeiss). ImageJ was employed for Z-stack/XY planes processing.

3.10 Methylation Specific qPCR (MSP-qPCR) in melanoma cells on IL-33 and IL-33 promoters

B16.F10 and A375M melanoma cells were seeded in 6 well plates (Corning) at a concentration of 5 x 10^5 in 2 ml of culturing medium. Mouse and human melanoma cells were treated with DAC 0.1 μM and 0.25 μM, respectively, or left untreated. After 24 h of culture, cells were harvested and genomic DNA was extracted from melanoma cells by Quick DNA™ MiniPrep (CAT N° D3024, Zymo Research, Irvine, CA, USA). Sodium bisulfite treatment of genomic DNA to convert unmethylated cytosine into uracil was carried out using EZ DNA Methylation™ Kit (Cat n° D5001, Zymo Research) according to manufacturer's instructions. MSP-qPCR primers were designed using the web tool MethPrimer (https://www.urogene.org/cgi-bin/methprimer/methprimer.cgi), sequences listed in Table S2). These primers were selected based on the presence of CpG islands, detected by The CpG Island search tool into the JavaScript toolbox Sequence Manipulation Suite (https://www.compgen.uni-muenster.de/tools/sms2/cpg_islands.html). Real time qPCR was performed on bisulfite converted cDNA with an Applied Biosystems™ 7500 Fast Real-Time PCR System (Life Technologies) by using the methylated or unmethylated primers pairs, which distinguish between methylated or unmethylated sequence of the P1 (mouse) or P (human) promoters. The *IL-33* gene sequence shows that there are three different promoter regions (P1, Promoter 2, and Promoter 3) positioned in different regions into this gene (Supplementary Fig. 2). We analyzed methylation status of a sequence into the P1 promoter (but not Promoter 2 and Promoter 3) sequence because of its optimal position at the 5' region of 3 *IL-33* isoforms (ENSMUST00000120388, ENSMUST00000144528, ENSMUST00000025724), spanning all the exons. Therefore, P1 sequence represents a potential suitable promoter for *IL-33* gene because of its upstream (5' region) location referring to the entire gene sequence, and also

covers the exon 1 (Supplementary Fig. 2). Similarly, the unique P promoter for two *IL-33* gene isoforms (ENST00000417746, ENST00000682010) is located upstream to the gene sequence and spans the *IL-33* exon 1 region (Supplementary Fig. 2). The conditions of real time MSP-qPCR reaction were as follows: 15 seconds at 95°C, 30 seconds at 60°C and 45 seconds at 72° for 40 cycles. The calculation of the methylation/demethylation status of human and murine *IL-33* gene promoters was carried out as previously described (Fazio C et al, 2019). Briefly, the percentage of methylation (% Meth) was defined as ratio between methylated fractions and the sum of methylated plus unmethylated fractions and data were reported as %. *Vice versa*, the percentage of demethylation (% Demeth) was defined as ratio between unmethylated fraction and the sum of methylated plus unmethylated fraction reported as %. The normalized %Meth and % Demeth percent values (Figure 5) refer to the analyzed *IL-33* P1 and *IL-33* P gene promoters (Supplementary Fig. 2).

3.12 Hanging drop spheroid method

A375M and SKMEL28 cells were cultured until confluence, trypsinized, and resuspended at a concentration of $1.65x10^5$/ml, respectively, in complete DMEM. The hanging drop method was applied to form tumor spheroids: cells were seeded as 30-µl drops in a homemade polydimethylsiloxane (PDMS) hanging drop membrane on the inverted lid of a 96-well plate and then placed at 37 °C in a humidified incubator under 5 % CO_2 atmosphere for 5 days.

3.13 Vascularized spheroid tumor model

Interactions between immune cells and the complex 3D vascularized TME were studied using a commercially available easy-to-use 3D tissue culture platform (OrganiX™, AIM Biotech). The platform comprises of 24 wells, each well containing a central gel region flanked by media channels on either side. The gel region contains the tumor spheroid cultured with vasculature in a collagen-fibrin gel network, and the media channels allow for the efficient delivery of nutrients and gas exchange.

The tumor spheroids were collected from the hanging drop membrane by centrifugation before being injected into the device. Thrombin stock was made at 100 U/ml and stored at - 80 °C. Aliquots of collagen stock (3.57 mg/ml) and fibrinogen stock (6 mg/ml) were prepared and stored at 4 °C and −80 °C respectively. A resuspension medium was prepared using thrombin (1 U/ml) and collagen (3.75 mg/ml) diluted from their stock solutions using cold EGM-2

media. Microvascular network were formed around the tumor spheroids using a co-culture of HUVEC and NHLF. HUVEC and NHLF were trypsinized, counted, and mixed in a resuspension medium at final concentrations of 8×10^6 HUVEC/ml and 2×10^6 NHLF/ml. The culture medium surrounding the tumor spheroids from hanging drops was completely removed and replaced with 25 µL of resuspension media containing the HUVEC-NHLF mixture. An equal volume of fibrinogen solution (6 mg/ml) was mixed with the spheroid and a total volume of 50 µL was aspirated and pipetted into the central gel region of the well. The fibrinogen, thrombin, and collagen mixtures were allowed to polymerize for 20 min at room temperature. After polymerization, EGM-2 supplemented with 50 µg/ml VEGF-A was added to the media channels for the first 3 days and changed daily. 4 days after device seeding, media were removed, and the side channels of devices with vascular networks were layered with 35 µl of HUVEC at 1×10^6 cells/ml and tilted at 45° on each side in the incubator for 15 min to allow formation of a HUVEC monolayer on the collagen-fibrin gel surface. Fresh EGM-2 medium was replenished in the reservoirs, and the devices were incubated at 37 °C in a humidified incubator under a 5 % CO_2 atmosphere. Three days after, PMBCs were added into the vascularized side channels in a concentration of $2x10^5$ cells in 35 uL and media with single treatment (DAC 0,25 uM, 100 ng/mL rhIL-33) and combination.

3.14 Confocal image acquisition of OrganiX and image analysis

All the subtypes of cells were stained previous the seeding into the Organix device. Melanoma cells A375M cells and SKMEL28 were labeled with the membrane dye PKH26 Red Fluorescence Cell Linker (MINI26, Sigma Aldrich). PBMCs were stained with DeepRed dye (Invitrogen ref. number C34565). GFP-HUVEC were used to allow the imaging of the vessels. All images were acquired on ZEISS LSM 800 and ZEISS LSM 880 confocal microscopes using Zeiss software, ZEN (blue edition).Z- stacks were acquired with a 150 um height with an interval of 3 um for each slice. PBMCs count and spatial orientation in the microenvironment were measured. Analysis was carried out using the FIJI ImageJ2 software.

3.15 Vessels phenotyping

Vessel formation was monitored and measured over 7 days. Pictures were taken on days 1, 4, and 7 post-seeding, and FIJI was used to generate summed z-projections to calculate vessel formation by measuring the percentage coverage over time. To analyze the effect of the

treatment on the vasculature network percentage of coverage area was measured as reported, after the 72h of treatment with DAC, IL-33 or the combination.

3.16 Flow cytometry from Organix

To establish the immune phenotype of the PBMCs inside the vascularized tumor model, after 7 days of culturing in the Organix and 72h hours of treatment, the cells were retrieved from the Organix to perform flow cytometry assay. The content of the main chamber was extracted from the bottom of the devices thanks to the plastic removable sticker. Next, the matrix-cell suspension was dissociated through an enzyme digestion process with an enzyme mix in serum free RPMI with Collagenase IV, Gibco (Stock 100mg/mL, use 1:10) Nattokinase, JBSL (Use 1:100) Trypsin 0.25% Gibco (Use 1:5) DNAse I, Merck (Use 1:200) for 6 min at 37 C to eliminate any presence of the matrix component. After the digestion, cells were incubated with LIVE/DEAD® Fixable Near-IR Dead Cells Stain Kit (Life technologies) and then labelled with fluorescent antibodies (mAbs). We used the following mAbs for T cell phenotyping: CD45 (Invitrogen YAML501.4), CD3 (BD Pharmaceutics, HIT3a) CD4 (BD Pharmaceutics, SK3) CD8 (BD Pharmaceutics, RPA-T8) CD25 (BD Pharmaceutic, M-A251) CD69 (Biolegend, FN50) PD-1 (BD Pharmaceutics, EH12.1) TIM3 (BD Pharmaceutics, 7D3).

3.17 RT-qPCR from Organix

After 7 days of culturing in the Organix and 72h hours of treatment, the cells were retrieved from the Organix to perform RT-qPCR assay. The content of the main chamber was extracted from the bottom of the devices thanks to the plastic removable sticker. Next, the matrix-cell suspension was dissociated through an enzyme digestion process with an enzyme mix in serum free RPMI with Collagenase IV (Stock 100mg/mL, use 1:10 Gibco) Nattokinase (Use 1:100 JBSL) Trypsin 0.25% (Use 1:5, Gibco) DNAse I (Use 1:200) to eliminate any presence of the matrix component. Finally, cells were resuspended in 300 uL of Triziol (Qiagen) to enable the cell membrane lysing. RNA from the cells was sequentially extracted with the RNA extraction with Quick-RNA^{TM} MiniPrep Zymo Research.

3.18 Statistical analysis

Mann-Whitney test was used for the nonparametric analysis of differences between two groups. One-way ANOVA analysis of variance followed by post hoc testing (Tukey) was used to compare means among multiples groups. Two-way ANOVA analysis of variance was used to

compare tumor growth curves. Log-rank Mantel-Cox test was used for the analysis of survival curves. Values were considered significant when the probability was below the 5% confidence level ($p \leq 0.05$).

4. RESULTS

4.1 Effect of combined treatment with Decitabine/IL-33 on melanoma growth

The first assessment of this study was to investigate the direct anti-tumor impact of DAC and IL-33 in single administrations or in combination on murine B16.F10 and human A375M melanoma cells. It is known that DAC has a double anti-tumor effect: at low concentration it works mainly as an epigenetic modifier, while at higher concentration it acts in a cytotoxic way, inducing apoptosis in cancer cells. MTS proliferation assay on 2D melanoma cells reinforced these finding revealing a strong dose-dependent anti-proliferative effect of DAC, independent of IL-33 treatment at different time points (24 h, 48 h, and 72 h post treatment) in both murine and human settings (Fig.. 1A, 1B). Moreover, we generated melanoma spheroids in ultra-low attachment wells to recapitulate the complex 3D tumor architecture. B16.F10 and A375M spheroids were cultured in the presence of IL-33 (100 ng/ml) and DAC (0.1 μM for murine cells, 0.25 μM for human) alone or in combination. The formation of melanoma spheroids was monitored through microscopy for six days. In the untreated control, a formation of defined spheroid was visible in both cell lines after four days (Fig. 2A, B). Interestingly, exposure to IL-33 alone did not affect the spheroid structure in either B16.F10 or A375M cells, as evidenced by similar Feret diameters and overall spheroid morphology (Fig. 2C, 2D).

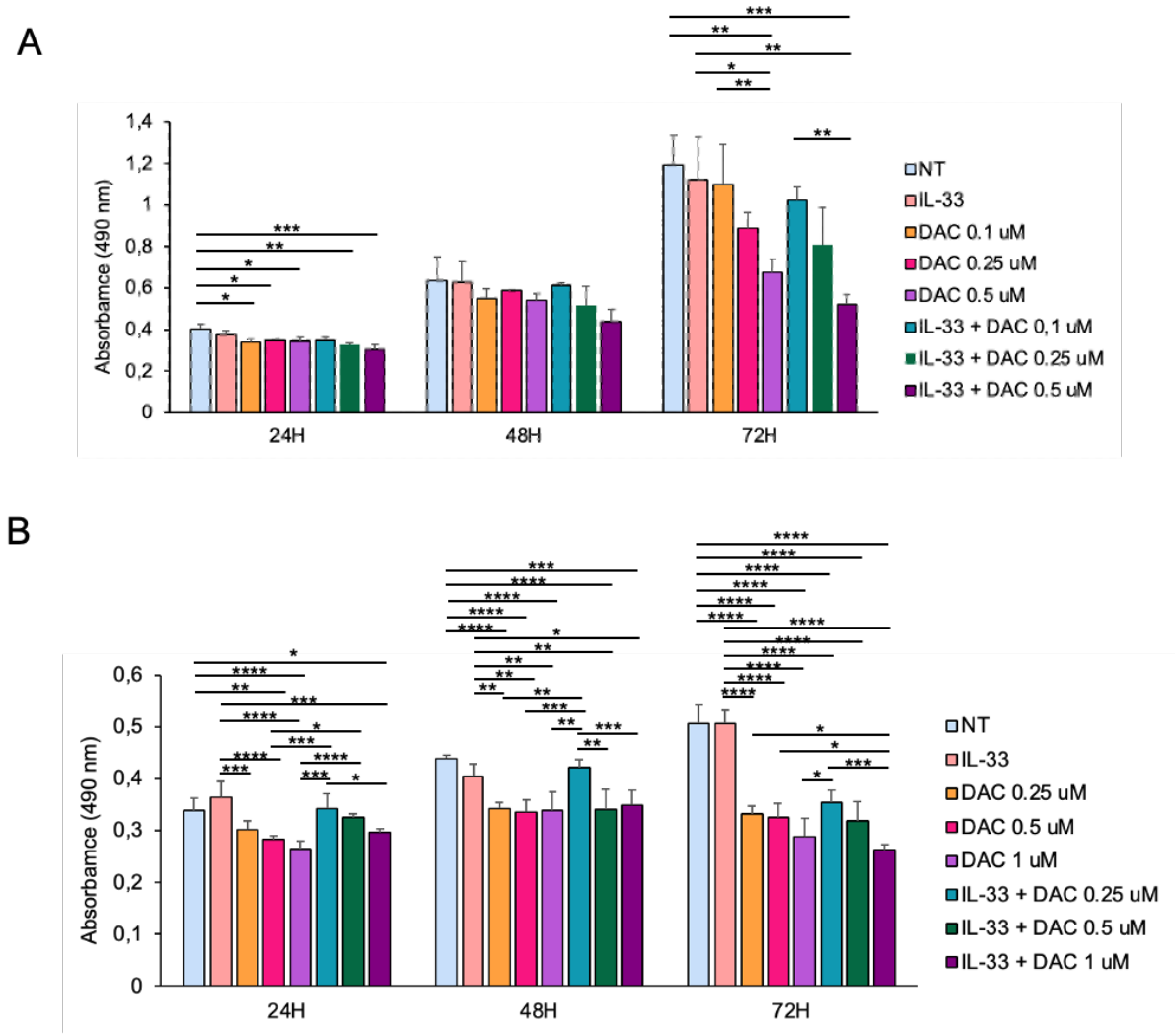

Figure 1. Viability assay of melanoma cells upon DAC, IL-33 or combinatory treatment. *MTS cell viability assay was performed on (A) B16.F10 melanoma cells were exposed to different conditions: alone (NT), in presence of rmIL-33 (100 ng/μL) and/or DAC at the indicated concentrations. Cell viability was evaluated at the indicated time points. Mean ± SD of three replicates is shown. (B) A375M melanoma cells were cultured alone (NT) or in the presence of rhIL-33 (100 ng/μL) and/or DAC at the indicated concentrations. Cell viability was evaluated at the indicated time points. Mean ± SD of five replicates is shown. *P<0.05, **P<0.01, ***P<0.001, ****P<0.0001.*

In contrast, the presence of DAC either as single agent or in combination with IL-33 significantly inhibited the formation of spheroid up to day six. (Fig. 2).

Thus, these analyses highlight the cytostatic activity of DAC and exclude the role of IL-33 as a direct antitumoral agent.

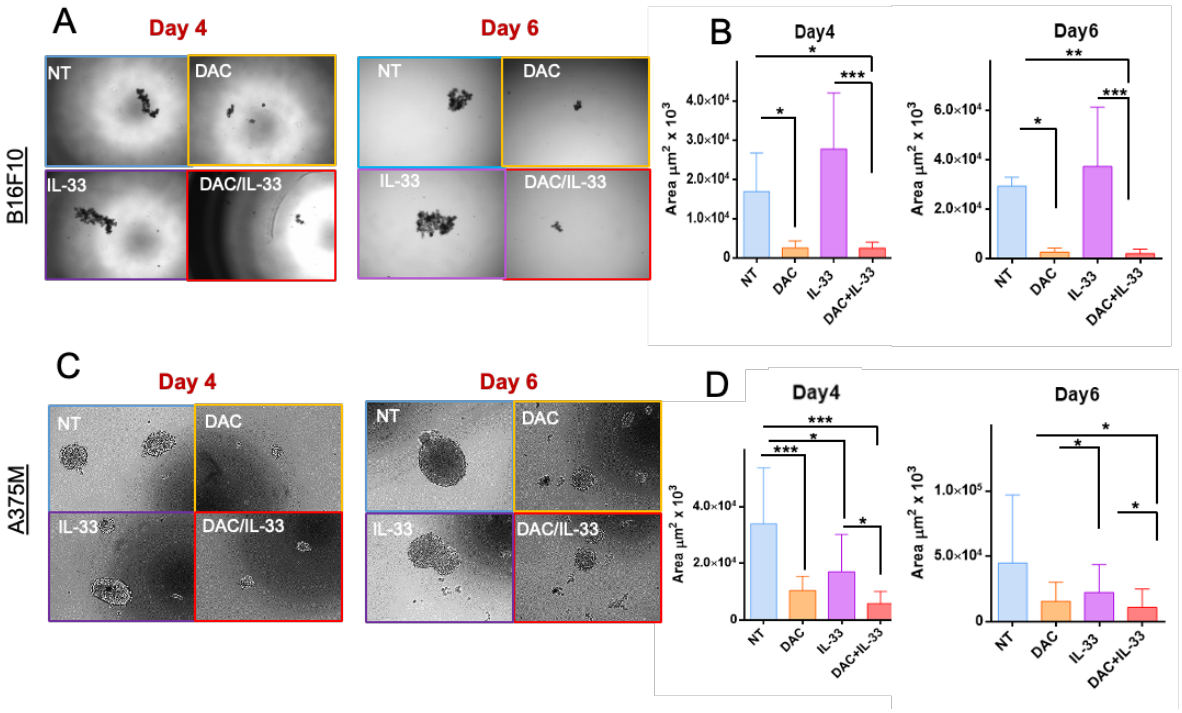

Figure 2. Direct effect of DAC in combination with IL-33 on melanoma spheroid growth. *(A) Murine B16.F10 melanoma cells were seeded on a 96-well ultralow attachment plates without treatment (NT) or in the presence of DAC (0.1 µM), rmIL-33 (100 ng/mL) or with the combination of DAC/IL-33. Microphotographs show the architecture of 3D spheroids after 4 and 6 days of culture time. (C) Human A375M melanoma cells were seeded on a 96-well ultralow attachment plates without treatment (NT) or in the presence of DAC (0.25 µM), rhIL-33 (100 ng/mL) or with the combination of DAC/IL-33. Microphotographs show the architecture of 3D spheroids after 4 and 6 days of culture time. On the right side, graphical representation of the analysis of the mean Feret diameter of each condition (5 replicates per condition) ± SD in (B) B16.F10 and (D) A375M spheroids.*P<0.05, ** P<0.01, *** P< 0.001.*

4.2 DAC and IL-33 synergize to promote T cell recruitment at the tumor site and to decrease melanoma growth in vivo

We next evaluated if DAC could enhance the anti-tumor activity of IL-33 *in vivo*. We divided the tumor bearing mice into four groups that received: i) a single injection of PBS (control group), ii) a single injection of DAC intraperitoneal (i.p.), iii) five consequentially injections of IL-33 intratumoral (i.t.), and iv) the combination of both (Fig 3A). Tumor volumes were measured at regular intervals and survival was monitored every three days. The combined administration of DAC plus IL-33 significantly reduced the tumor growth relative to the control mice (Fig 3B). However, tumor growth inhibition in mice receiving the combo treatment did not significantly diverge from that in mice exposed to the single treatments. Despite

this,survival analysis revealed a more interesting outcome, due to the fact that the DAC/IL-33 effect ameliorated more significantly the survival rates in mice compared to the control and single treatments (Fig 3C).

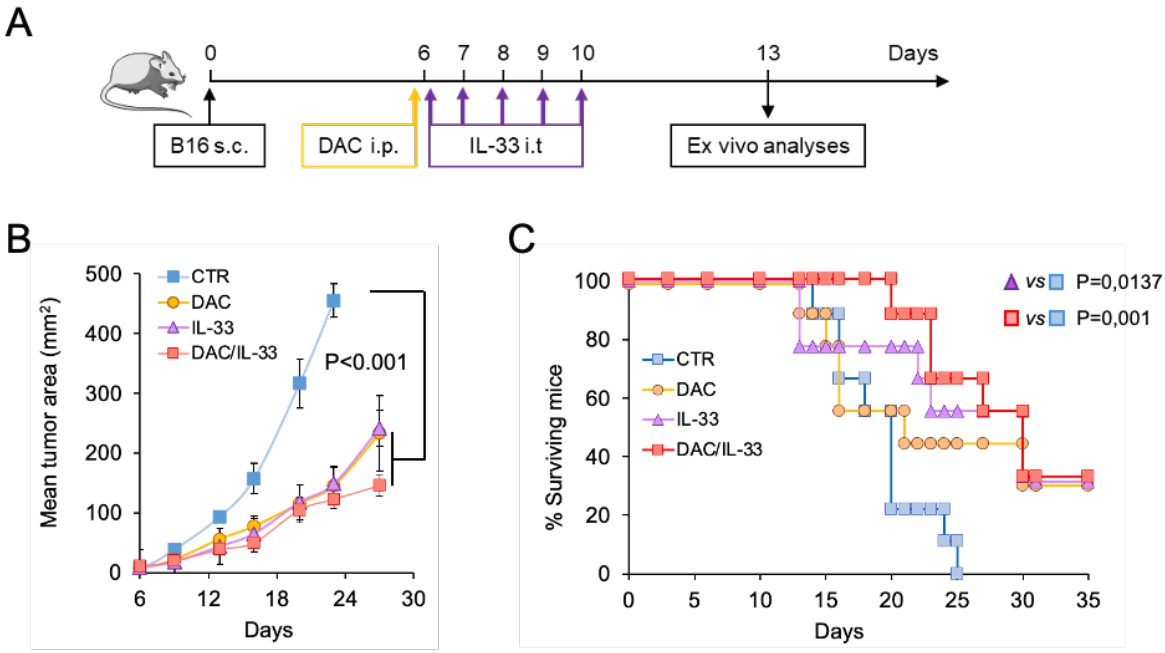

Figure 3. DAC/ IL-33 combined treatment efficacy in vivo *(A) Schematic representation of the workflow for the in vivo setting. C57BL/6 mice were injected subcutaneously with B16.F10 melanoma cells (0.8 x 105) and treated with DAC (1 mg/kg i.p.), IL-33 (0.4 µg/mouse i.t.) singly or combined. PBS was administered to the Control mice group (CTR). Ex vivo analyses were carried out on day 13. (B) Tumor growth showed in the different groups. Mean tumor area of individual mice (n=9) ± SD is shown. (C) Kaplan Meier Plot representing percentage of surviving mice within each group. Data represent the mean value of individual mice (n=12-16) ± SD. *P<0.05, ** P<0.01, *** P< 0.001, ****P<0.0001*

To investigate any changes in the immune TME, flow cytometry on the immune infiltrate was performed 3 days after the last administration of IL-33. We discovered that the tumor tissue from mice treated with DAC/IL-33 displayed a more abundant recruitment of CD45+ leucocytes (Fig 4A). Compared to single treatments, combined DAC/IL-33 induced significant increase in tumor-infiltrating CD4+ and CD8+ T cells and of eosinophils with respect to control mice (Fig. 4A). Interestingly, the percentage of tumor-infiltrating eosinophils in melanoma from combo- treated mice was significantly higher also with respect to single treatments. In contrast, granulocytic myeloid derived suppressor cells (G-MDSC) remained unchanged across the treatments (Fig. 4A). The qRT-PCR analysis show that DAC and IL-33 synergize to increase the Th1-related effector molecules, like granzyme B (GZMB) IL-12, and the T cell-

attracting chemokine CCL5 in the TME (Fig. 4B). These data highlight the synergistic effects of DAC and IL-33 in shaping the immune TME orchestrating an expanded and activated immune landscape.

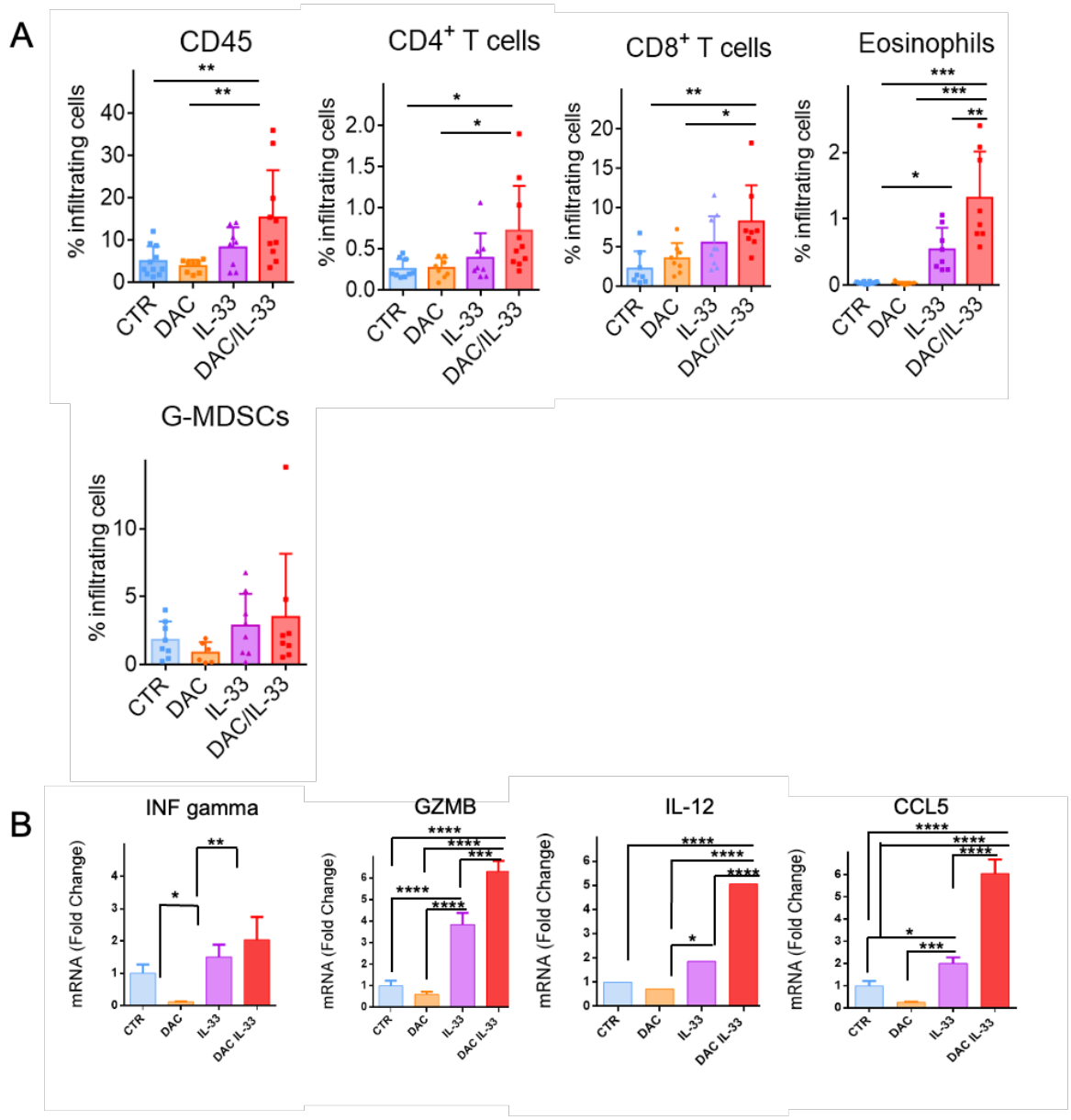

Figure 4. Phenotyping of the different immune subpopulation recruited after DAC/IL-33 treatment in vivo *A) Flow cytometry analysis shows the immune cells milieu infiltrating in the TME in response of the different treatment. B) Chemokine and cytokine expression in tumors mice infiltrates by real time q- PCR. Sample were analyzed at day 13. Data shown the mean value of individual mice (n=7-12) ± SD. *P<0.05, ** P<0.01, *** P< 0.001, ****P<0.0001*

To further analyze this immune TME, we performed gene expression analysis of immune checkpoints relevant for targeted immunotherapies (i.e., PD-1, TIGIT, LAG-3 and Tim-3). We observed that DAC and IL-33 synergistically upregulated the expression of PD-1 in melanoma tumors (Fig. 5A). In contrast, the other immune checkpoint molecules analyzed such as TIGIT, Tim-3 and LAG-3 were not significantly upregulated by the combo treatment with respect to the single treatments (Fig. 5A). Through flow cytometry, we confirmed significantly higher percentages of PD-1-expressing CD4+ and CD8+ T cells in tumors from mice receiving DAC/IL-33, but not from those receiving single treatments, with respect to controls (Fig. 5B). In contrast, the surface expression of TIGIT, Tim-3 or LAG-3 in either CD4 or CD8 T cells was unaffected by any treatment (Fig. 5C).

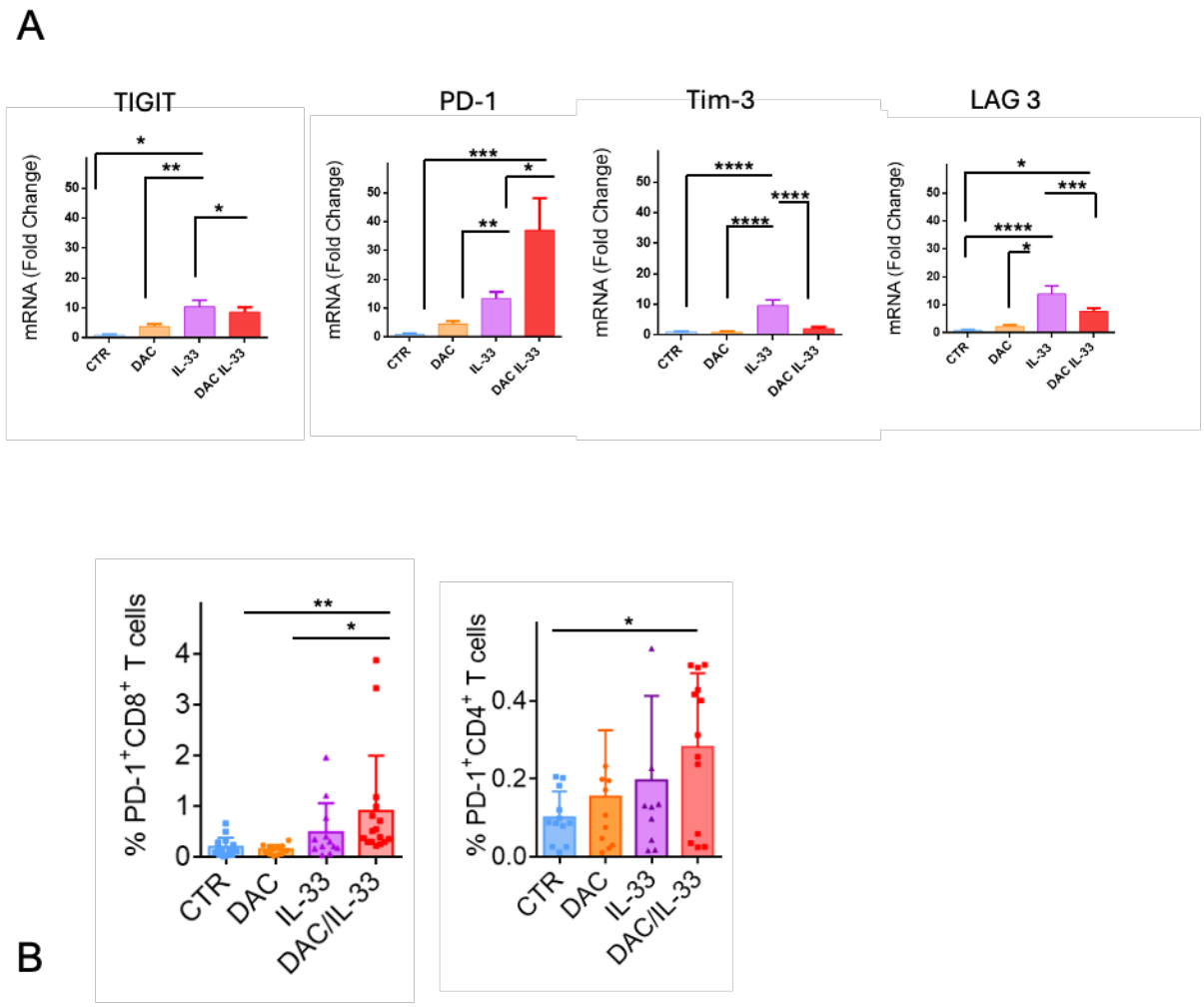

***Figure 5*. Molecular analysis of the immune infiltrate *in vivo*.** *A) Immune checkpoints expression in mice tumors infiltrate by real time q- PCR. Data are expressed as mean fold change of mRNA expression vs control of individual mice. B) Flow cytometry data of PD-1 surface expression in CD8+*

*and CD4+ T cell (n=7) ± SD in mice tumor. Data represent the mean value of individual mice (n=12-16) ± SD. *P<0.05, ** P<0.01, *** P< 0.001, ****P<0.0001*

4.3 DAC requires IL-33/ST2 axis for anti-tumor efficacy

In the TME, IL-33 is expressed by epithelial cells, fibroblast and tumor cells (Cayrol 2018). Moreover, endogenous IL-33 appears to have an anti-tumor effect in various cancer models, including colorectal cancer (Chen et al 2020), PDAC (Dixit et al 2022), breast cancer and melanoma (Gao et al 2015; Lucarini et al 2017). We sought to examine whether the possible mechanism underling the cooperation of DAC and IL-33 was related to the requirement of IL-33/ST2 axis for DAC to exploit its anti-tumor activity *in vivo*. To achieve this goal, we tested the anti-tumor efficacy of DAC in mice deficient of the ST2 receptor ($ST2^{-/-}$). WT and $ST2^{-/-}$ mice bearing palpable B16.F10 melanoma tumors were treated with DAC or other anti neoplastic drug cisplatin (CDDP) or the immunogenic drug doxorubicin (DOXO), as comparison controls. All drugs were able to significantly delay tumor growth in WT mice (Fig. 6A). Noticeably, while CDDP and DOXO were effective in both the WT and $ST2^{-/-}$ mice, the anti-tumor action of DAC was completely abrogated in $ST2^{-/-}$ mice (Fig. 6B). These data indicate that DAC requires IL-33/ST2 signaling to exert its anti-tumor activity.

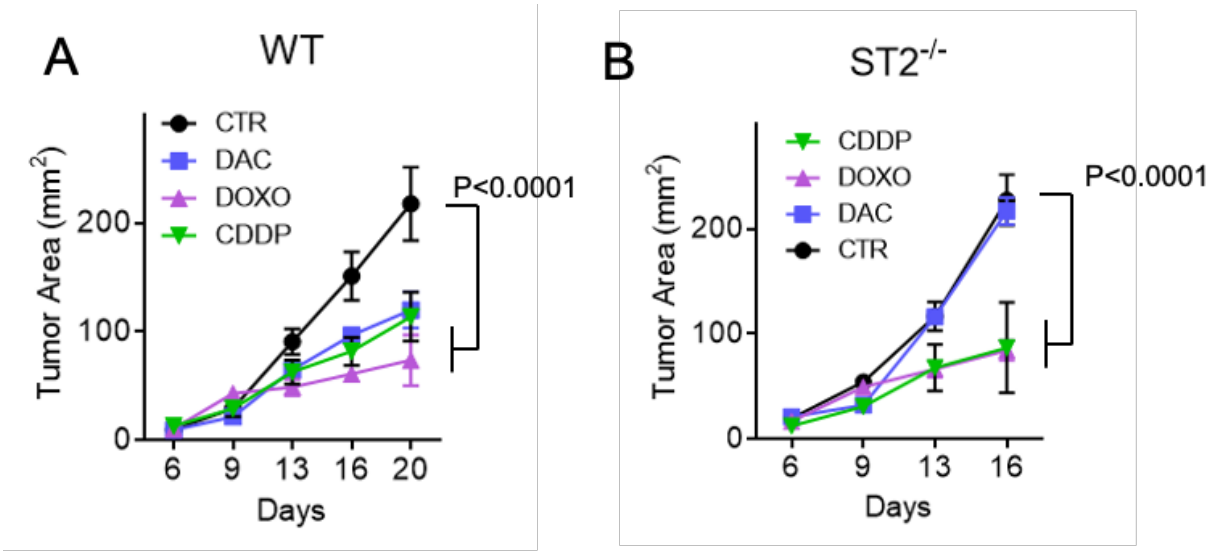

Figure 6. Role of the endogenous IL-33 in the antitumor efficacy of DAC*. Graphical representation of the tumor growth in (A) C57BL/6 wild-type (WT) and (B) ST2-/- mice implanted with B16.F10 melanoma cells (0.8 x 105) were treated with DAC (1 mg/kg i.p.), CCDP (2.5 mg/kg i.t.) or DOXO (2 mM i.t.). Mean tumor area of individual mice (n=5-10) ± SD is shown.*

To better understand the mechanism(s) underlying the requirement of IL-33/ST2 signaling for DAC anti-tumor efficacy, we explored whether this epigenetic drug positively modulates this axis *in vivo*. To this end, we analyzed the expression of IL-33 and ST2 in the TME of WT mice early after DAC treatment (3 days post injection). We found a significantly increased expression of both IL-33 and ST2 mRNAs in tumors from mice exposed to DAC treatment compared to the control group (Fig. 7), suggesting a DAC-dependent positive feedback mechanism.

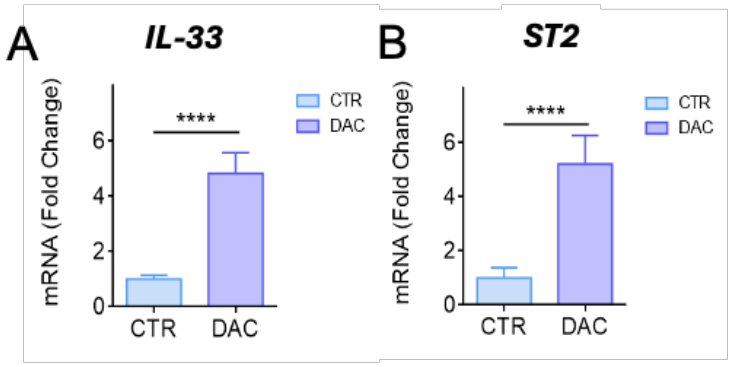

Figure 7. DAC improve the IL-33 and ST2 molecular expression in melanoma mice tumors. Expression of *IL-33* and *ST2 in melanoma tumors of C57BL/6 WT mice 3 days after DAC treatment. Data are expressed as mean. fold change of mRNA expression vs control of individual mice (n=5) ± SD. ****P< 0.0001.*

To evaluate whether the IL-33/ST2 upregulation by DAC was required for inducing immune recruitment, we investigated the immune infiltrate within the TME from WT mice and ST2$^{-/-}$ at the same time point. We noticed an increase in the frequency of CD4+ and CD8+ T cells as well as eosinophils selectively in DAC treated WT mice, but not in the ST2-/- counterparts (Fig. 8A). Moreover, gene expression analysis showed that chemokines attracting T cells, such as CCL5, CXCL9, and CXCL10, as well as eosinophil-recruiting chemokines like CCL11, were upregulated in tumors from DAC-treated WT mice.
In contrast, this upregulation was not observed in ST2$^{-/-}$ mice, which well correlates with the distinct immune landscape found in the TME of the two mouse strains (Fig. 8B).

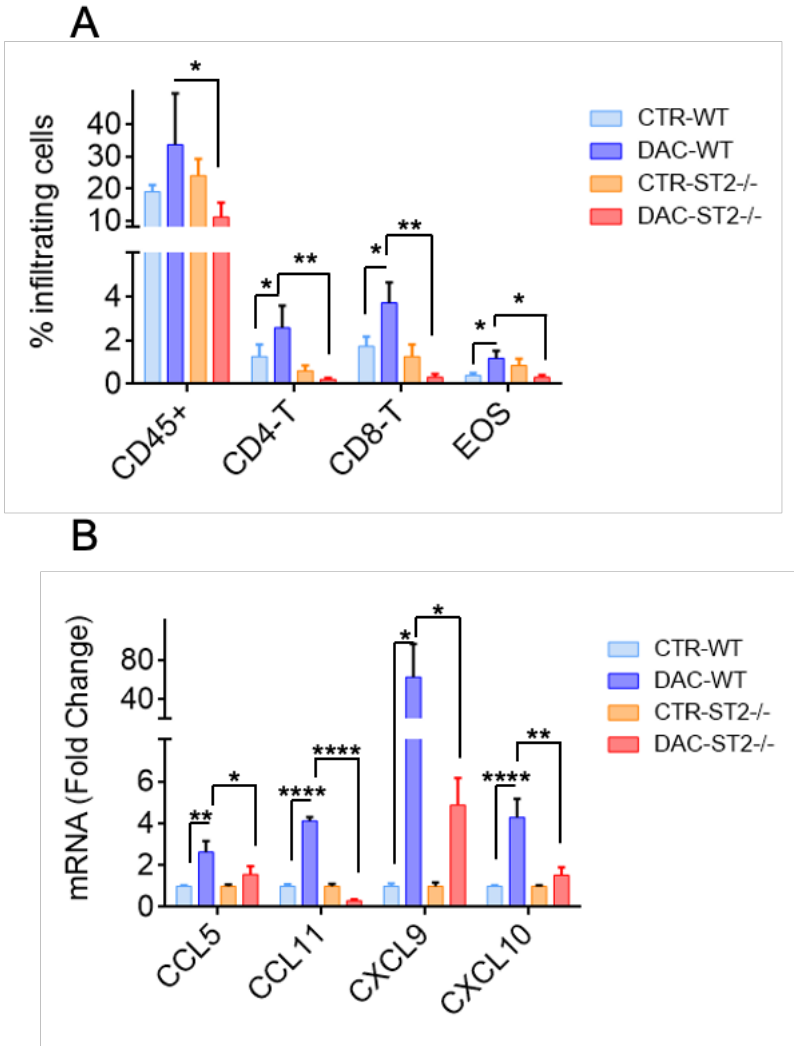

Figure 8 Analysis of the immune subset in the TME of WT and ST2-/- mice after DAC treatment. *Flow cytometry data shows the differences in the recruitment of immune infiltrates in (A) C57BL/6 WT and ST2-/- mice. Samples were analyzed 3 days after DAC treatment. Data show the mean value of individual mice (n=5) ± SD. (B) Expression of indicated chemokines in melanoma tumors C57BL/6 WT and ST2-/- mice 3 days after DAC. Data are expressed as fold change of mRNA expression vs control of individual mice (n=5) ± SD. *P<0.05, ** P<0.01, *** P< 0.001 ****P<0.0001.*

Taken together, these findings suggest that the anti-tumor activity of DAC does not only rely in suppressing tumor proliferation, but also in its ability to shape the tumor-immune crosstalk through the induction of the IL-33/ST2 axis, which therefore could orchestrate the immune recruitment in the TME.

4.4 DAC epigenetically activates IL-33 gene expression in melanoma cells by demethylating its gene promoter

Mechanistically, DAC is known to regulate gene expression through hypomethylation of promoters of genes when given to low-dose concentration. (Giunta EF. et al 2020). Since it is well established that tumor cells can be a source of IL-33, we wanted to investigate if the increment of IL-33 in TME of mice treated with DAC correlated with epigenetic modifications by DAC on melanoma cells to induce IL-33 expression. We confirmed that the exposure of DAC upregulated IL-33 expression in B16.F10 murine and A375M human melanoma cells *in vitro* in a dose-dependent manner (Fig. 9A).

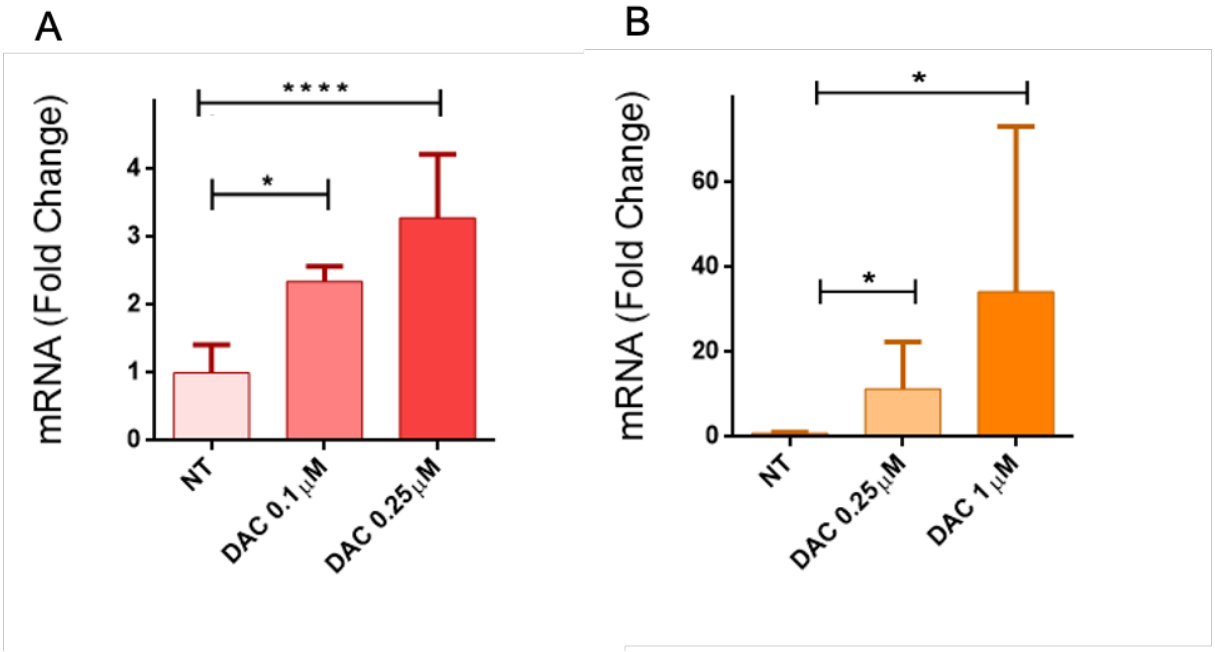

Figure 9 In vitro IL-33 expression in mouse and human melanoma cells after DAC treatment*. In vitro IL-33 mRNA expression in A) B16F10 murine cells and B) A375M human cells after exposure increasing dosage of DAC. Histograms represent mean fold change of mRNA expression vs control in culture replicates ± SD. *P< 0.05, **** P< 0.0001*

The hypomethylating activity of DAC occurs specifically on the CpG island on gene promoters. To assess if this epigenetic drug had a direct mechanism of action on the IL-33 gene, we conducted methylation specific-qPCR assays on the promoters of murine and human IL-33 gene. By specific MGI Genome Informatics webtools, we first identified the P1 DNA sequence

as the promoter of mouse B16.F10 melanoma cells (Fig. 10A) and the P DNA sequence as the prometer for the human A375M cells (Fig. 10B).

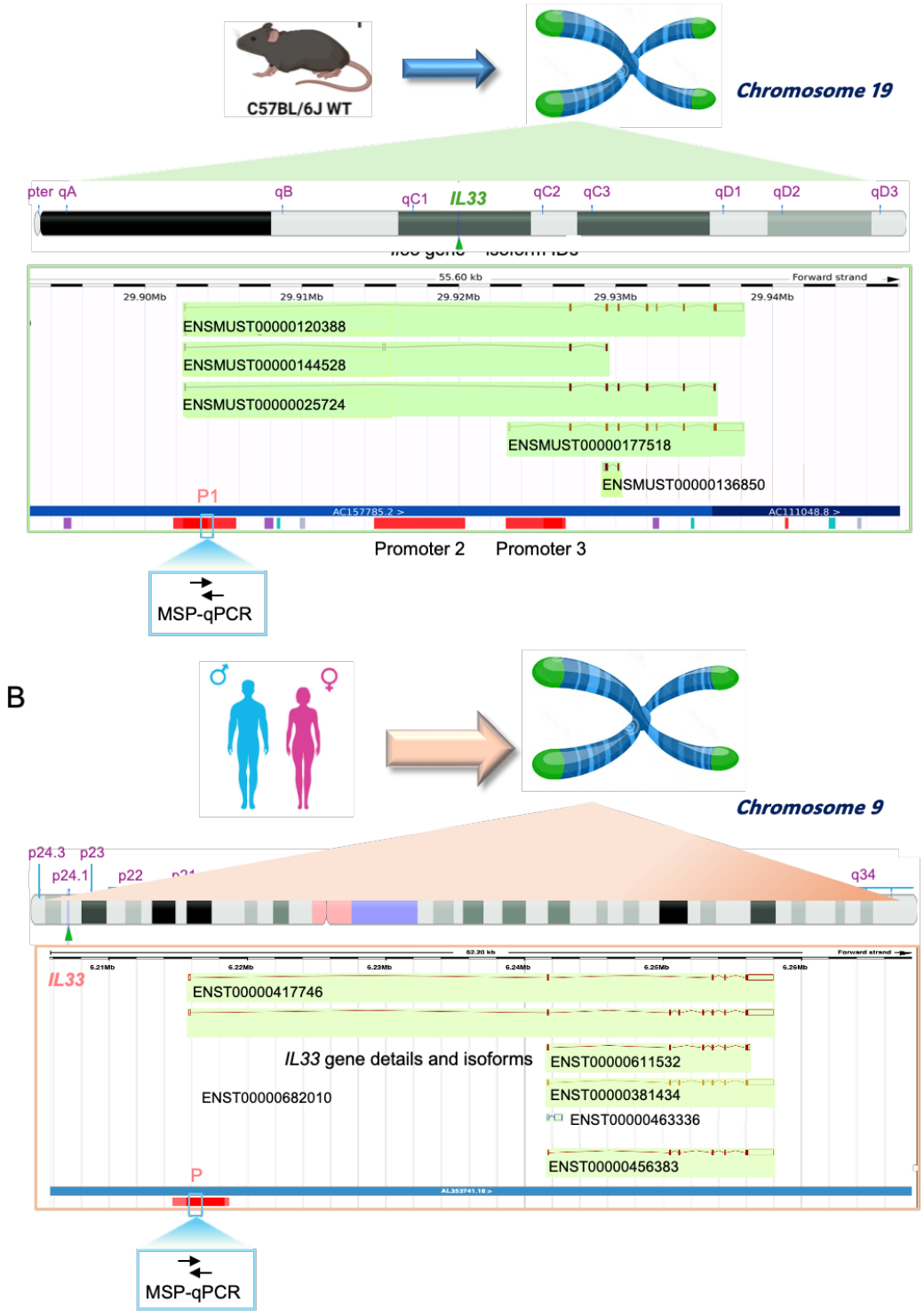

Figure 10 Graphical representation of the mouse and human IL-33 gene promoters assayed by MSP-qPCR. *Localization map for (A) mouse and human IL-33 gene promoters on Chromosome 19 and Chromosome 9 respectively employed in the methylation qPCR. The blue rectangle indicates the amplicon of the examined promoter, generated by the forward and reverse primers used to study their*

methylation status. Chromosome maps exhibit in the upper part of each figure are based on the conventional cytogenetic band nomenclature showing position of gene promoters in mouse (A, IL-33 P1 promoter sequence in qC1 region inside the long arm of Chromosome 19) and human (B, IL-33 P promoter sequence in p24.1 region inside the short arm of Chromosome 9). Chromosome maps have been generated by the Genome Data Viewer (National Library of Medicine, https://www.ncbi.nlm.nih.gov/gdv/). Graphical maps of gene isoforms and their promoter sequences have been obtained by the ENSEMBL webpage tool (https://useast.ensembl.org/index.html) via the Gencode database version 46 (released in May 2024). P1, mouse IL-33 promoter sequence; P human IL-33 promoter sequence. Brown boxes, exons. Red boxes, promoter sequences.

We observed significant demethylation of the P1 *IL-33* gene promoter in B16.F10 melanoma cells after 24 h of exposure to DAC (0.1 μM) compared to the untreated control (Fig. 11A). Similarly, a decreased percentage of methylation and an increased de-methylation of the P *IL-33* gene promoter, was found in A375M cells after 24 h treatment with DAC (0.25 μM) compared to untreated cells (Fig. 11B).

These data suggest that DAC epigenetically reactivates IL-33 gene in tumor cells via demethylation of its specific upstream promoter sequence and that the functional endogenous IL-33/ST2 axis is required for its anti-tumor activity.

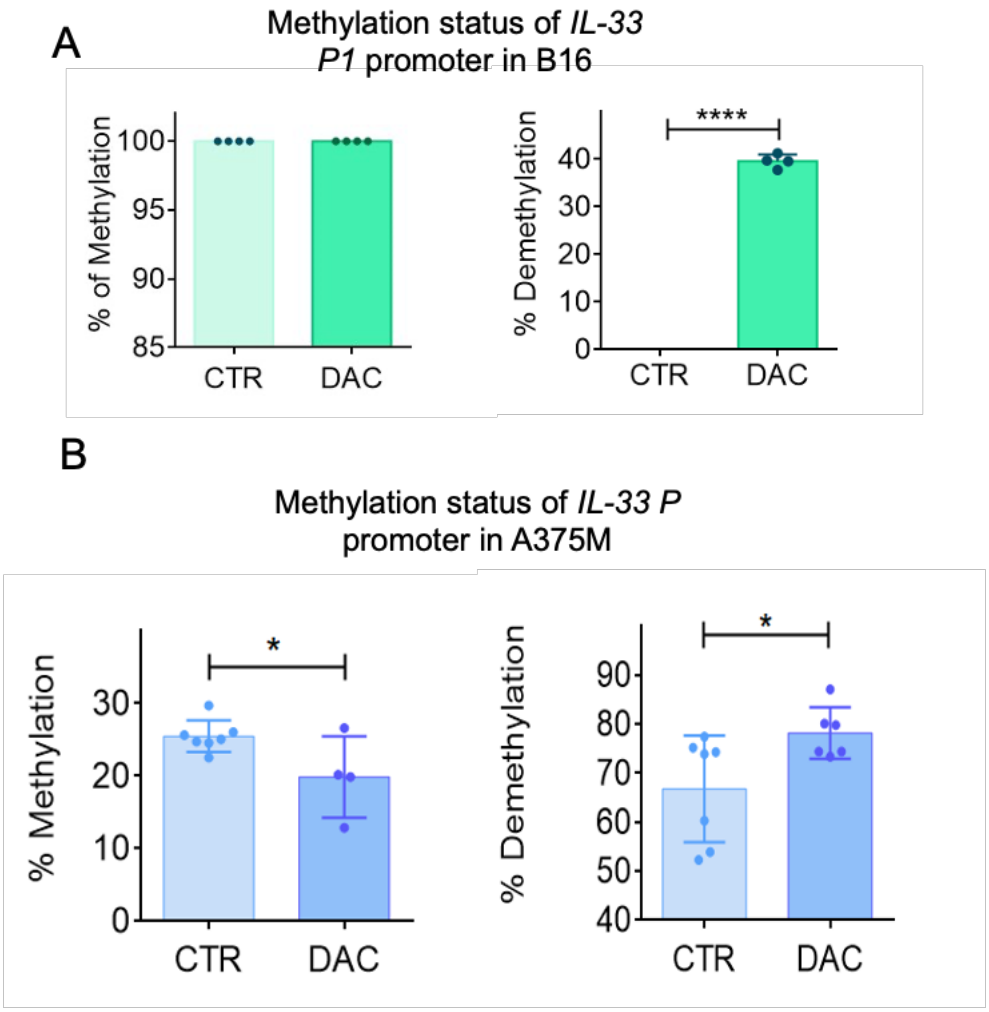

Figure11. Mechanism of action of DAC. Epigenetic regulation of IL-33 promoters.. *Methylation specific qPCR shows the mechanism of action by which DAC operates on IL-33 expression. Histograms show the differences in the % of methylation and de-methylation of IL-33 gene promoters status on mouse (A) B16F10 and human (B) A375M melanoma cells after 24h of exposure to DAC 0,1uM and 0,25 uM respectively compared to control condition (CTR) *P<0.05, ****P<0.0001.*

4.5 3D microfluidic chip assays reveal that DAC and IL-33/ST2 axis cooperate to promote immune cell recruitment to the tumor site

Our *in vivo* experiments suggest that DAC co-operates with the IL-33/ST2 axis to foster immune cell recruitment in the TME. To further evaluate the combinatory action of DAC and IL-33 in promoting tumor-immune crosstalk we employed an OoC technology that relies on a 3D microfluidic chip-based approach.. OoC models are a valuable resource into the more

specific analysis and implies new advantages into the manipulation of the TME and the possibility of a deeper analysis of the immune tumor crosstalk (Mattei 2021; Moresi et al. 2025). We established a dual TME competitive 3D migration assay to analyze the ability of the immune cells to selectively migrate to a TME exposed to the combo DAC/IL-33 compared to the opposite TME, exposed to the single treatment or to control (Lucarini V. et al,2017). For our specific purposes, we used an *ad hoc* fabricated microfluidic device where B16.F10 melanoma cells, previously labeled with a PKH67 green dye, were embedded in a Matrigel matrix in the presence or absence of IL-33, DAC or combo (Fig 12A-B).

These Matrigel-embedded melanoma cell preparations were seeded in two lateral chambers that are connect to main one with a series of micro channels that allows cell migration. Splenocytes from naive either WT or ST2-/- mice labeled with a PKH26 red dye were resuspended in RPMI media and inserted in the central chamber (Fig 12A,B). The preferential migratory behavior of immune cells towards the left or right melanoma chambers in a competitive fashion was then evaluated by fluorescence microscopy at various times of culture (Fig 12A,B).

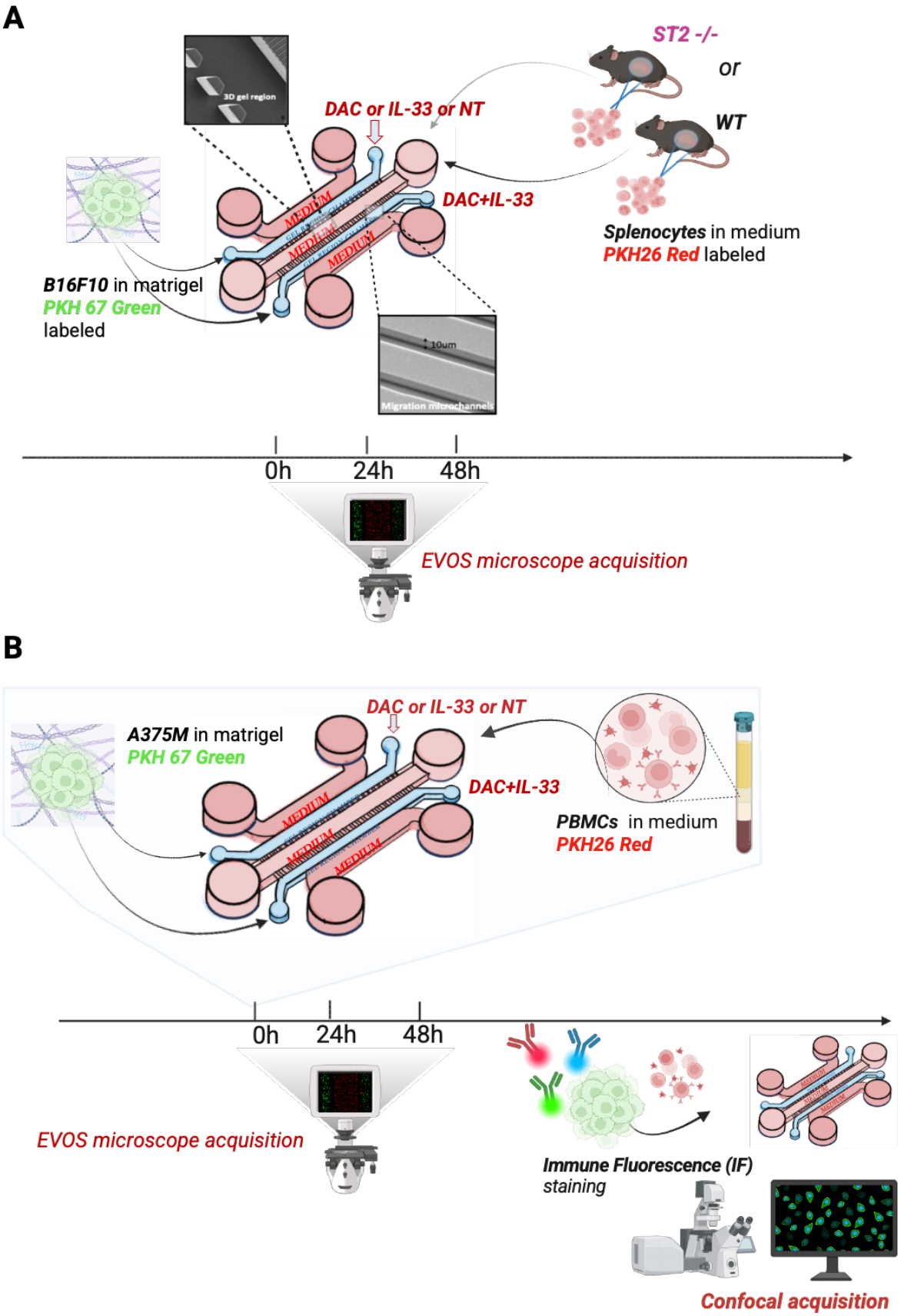
A
ST2 -/-
or
WT
3D gel region
DAC or IL-33 or NT
DAC+IL-33
MEDIUM
Splenocytes in medium
PKH26 Red labeled
B16F10 in matrigel
PKH 67 Green
labeled
10um
Migration microchannels
0h
24h
48h
EVOS microscope acquisition
B
A375M in matrigel
PKH 67 Green
DAC or IL-33 or NT
DAC+IL-33
PBMCs in medium
PKH26 Red
0h
24h
48h
EVOS microscope acquisition
Immune Fluorescence (IF)
staining
Confocal acquisition

Figure 12. Schematic representation of the competitive migration microfluidic devices assay. *(A) B16F10 prior labeled with PKH67 green, were loaded in the gel region chambers embedded in Matrigel. Matrigel melanoma cells mix exposed to DAC+IL-33 treatment was kept on the right gel chamber while on the left side were alternatively inserted the other condition of DAC and IL-33 alone or not treated cells. Solenocytes from either wild type or ST2 -/- mice PKH26 red labeled were loaded in the main chamber in RPMI medium resuspension. EVOS micro-photograph were acquired st 0h, 24h and 48h post seeding. (B) Same experimental assessment was kept during the seeding of human A375M and PBMCs inside the device. After the last time point (48h), cells were fixed and stained with immune fluorescence antibodies and acquired at the confocal microscope.*

When WT splenocytes were used as responders, a preferential migration towards the right chamber containing melanoma cells exposed to DAC/IL-33 combo treatment as opposed to the left chamber containing single treated (IL-33 or DAC) or untreated melanoma cells was observed at 48 h of culture (Fig. 13A).

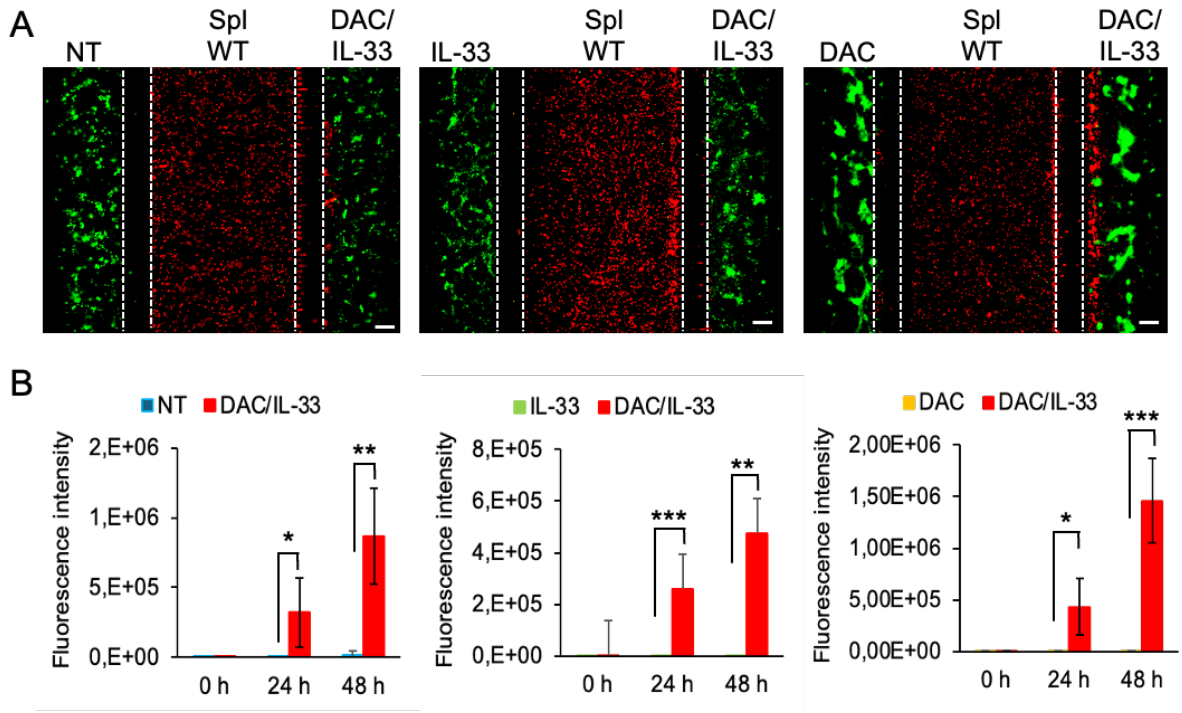

Figure 13. Competitive migration in microfluidic device shows the cooperative action of DAC and IL-33 in the recruitment of splenocytes.

A) Microfluidic devices were used to analyze the competitive migration of splenocytes from C57BL/6 WT mice towards melanoma cells exposed to DAC/IL-33. PKH26-labeled (red) spleen cells resuspended in RPMI medium were loaded in the central chamber of microfluidic devices.

PKH67-labeled (green) B16.F10 melanoma cells embedded in Matrigel containing the treatments were placed in lateral chambers. Each device has the setting with DAC/IL-33 condition confronted with untreated condition (NT, left), IL-33 alone (central) or DAC alone (right). Fluorescence images acquired through the EVOS microscope were obtained after 48 h of culture.
*Red fluorescence represents displacement of (A) WT spleen cells towards melanoma chambers (green) containing the indicated treatments. Discontinued vertical white lines depict microchannel area. Scale bars = 1000 μm. B) Quantitative analysis of red fluorescence intensity in the tumor chambers reflecting the preferential migration of WT spleen cells towards DAC/IL-33 treated vs the other condition as displayed. Data show the mean ± SD of several fields of at least 3 devices per experimental condition. *P<0.05, ** P<0.01, *** P< 0.001*

Quantitative red fluorescence analysis in the two melanoma chambers, confirmed higher presence of splenocytes migrated into the DAC/IL-33 conditioned TME starting from 24 h (Fig. 13B). In contrast, when ST2-/- splenocytes were used, no significant migration was observed toward either combo treated or single treated melanoma cell chambers at any time point (Fig. 14A, B).

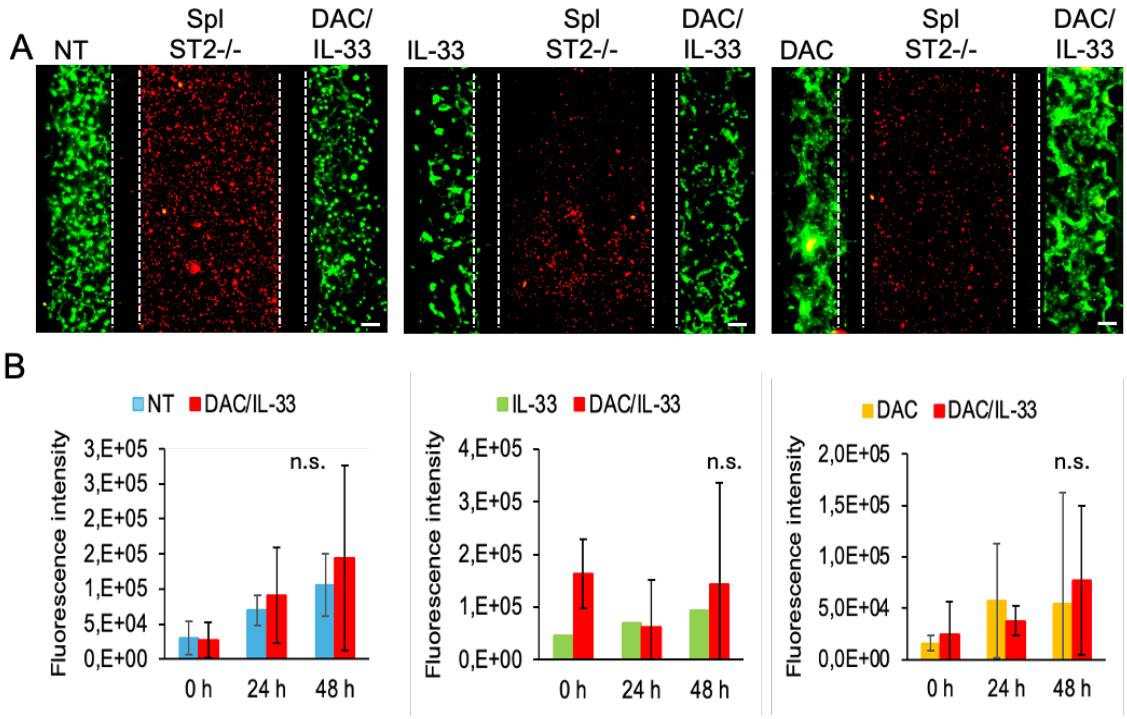

Figure 14. DAC and IL-33/ST2 axis cooperate to promote tumor-immune crosstalk in a 3D microfluidic system

Microfluidic devices were used to analyze the competitive migration of splenocytes from C57BL/6 ST2-/- mice towards melanoma cells exposed to DAC/IL-33. PKH26-labeled (red) ST2-/- spleen cells resuspended in RPMI medium were loaded in the central chamber of microfluidic devices.

PKH67-labeled (green) B16.F10 melanoma cells embedded in Matrigel containing the treatments were placed in lateral chambers. Each device has the setting with DAC/IL-33 condition confronted with untreated condition (NT, left), IL-33 alone (central) or DAC alone (right). Fluorescence images acquired through the EVOS microscope were obtained after 48 h of culture.
*Red fluorescence represents displacement of ST2-/- spleen cells towards melanoma chambers (green) containing the indicated treatments. Discontinued vertical white lines depict microchannel area. Scale bars = 1000 μm.B) Quantitative analysis of red fluorescence intensity in the tumor chambers reflecting the preferential migration of ST2-/- spleen cells towards DAC/IL-33 treated vs the other condition as displayed. Data show the mean ± SD of several fields of at least 3 devices per experimental condition. *P<0.05, ** P<0.01, *** P< 0.001*

These findings indicate that IL-33/ST2 is an essential molecular axis for immune migratory response to DAC.

We next translated this observation to a human setting by assessing the preferential migration of PMBCs from healthy donors towards A375M melanoma cells exposed to combo, single treatments or untreated in microfluidic chips. As expected, we observed a clear preferential migration of PBMCs toward the DAC/IL-33 melanoma chamber as opposed to the single-treated or untreated cell chambers at 24 h and, more markedly, at 48 h of co-culture (Fig. 15 A, B).

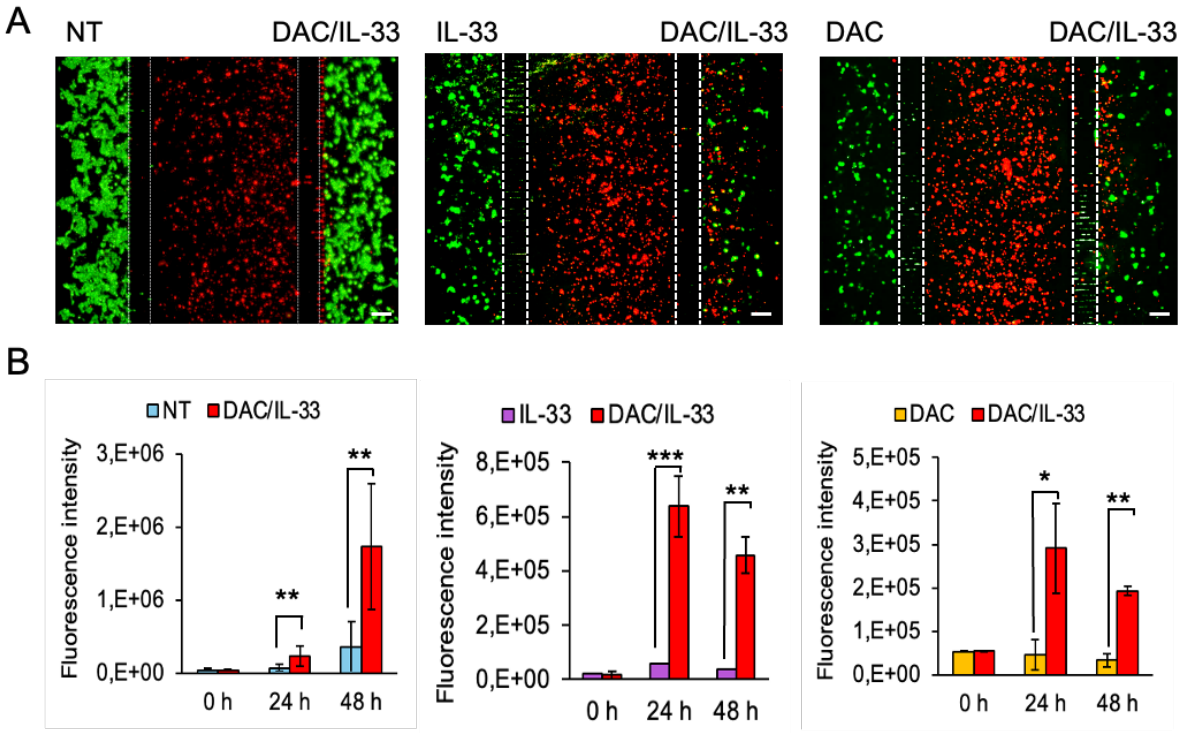

Figure 15. DAC and IL-33 cooperates in the recruitment of PBMCS in a huma 3D micrfuidic assay setting.

*Competitive migration assay of PBMCs towards DAC/IL-33 treated A375M melanoma cells in a 3D microfluidic chip. PKH26-labeled (red) PBMCs were loaded in the central chamber of microfluidic devices. PKH67-labeled (green). A375M melanoma cells embedded in Matrigel containing the treatments were placed in lateral chambers. In every device the condition DAC/IL-33 was confronted with not treated condition (NT, left), IL-33 alone (central) or DAC alone (right). Fluorescence images were obtained after 48 h of culture. Red fluorescence represents displacement of PBMCs towards melanoma chambers (green) containing the indicated treatments. Discontinued vertical white lines depict microchannel area. Scale bars = 100 μm. (B) Quantitative analysis of red fluorescence intensity in the tumor chambers reflecting the preferential migration PBMCs towards DAC/IL-33 treated vs untreated (left), IL-33 treated (middle) or DAC treated (right) melanoma cells. Data show the mean ± SD of multiple fields of at least 3 devices per experimental condition. *P<0.05, ** P<0.01, *** P< 0.001.*

To identify effector immune populations, we stained the PBMCs migrated in the DAC/IL-33 treated A375M melanoma gel chambers. Confocal microscopy showed the presence of several CD8+ T cells in the DAC/IL-33 melanoma chamber in strict proximity of tumor cells. Conversely, rare or no CD8+ T cells were found in the gel chambers containing A375M cells treated with either DAC or IL-33 alone or left untreated (Fig. 16A, B, C). Overall, these OoC-based assays findings show the cooperation of DAC and IL-33 in promoting immune cell recruitment, including CD8+ T cells, also in the human setting accordingly of the results obtain in the *in vivo* setting.

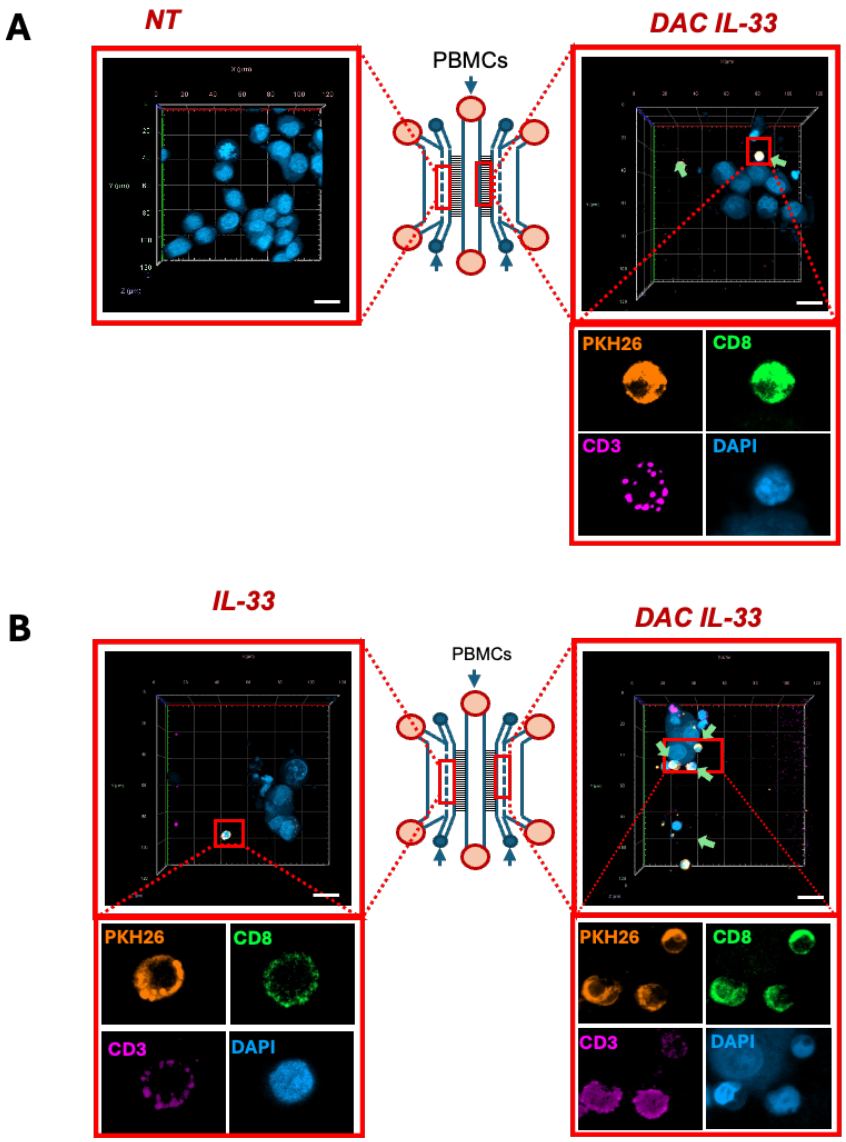
A
NT
PBMCs
DAC IL-33
PKH26
CD8
CD3
DAPI
B
IL-33
PBMCs
DAC IL-33
PKH26
CD8
CD3
DAPI
PKH26
CD8
CD3
DAPI
C
DAC
PBMCs
DAC IL-33
PKH26
CD8
CD3
DAPI
PKH26
CD8
CD3
DAPI

Figure 16. DAC/IL-33 increase the recruitment of CD8+ T cells towards A375M melanoma cells in a 3D microfluidic system

Bird's eye view of the 3D microfluidic chip used for the competitive assay experiments. 3D confocal reconstruction in microfluidic system. Z stack of each different experimental condition was acquired with a 20X magnification. Specific ROI were later analyzed to to investigate the presence of CD8+ infiltrates. DAC-33 chamber shows a higher number of CD8+ positive PBMCs infiltrates in compared to NT (A), where no relevant PBMCs infiltration was present. IL-33 (B) shows a smaller number of CD8+ cells interacting with the tumor compared to DAC-33 and lastly in DAC condition (C) PBMCs CD8- an CD3- negative were the only one interacting with the tumor. Scale bar 20 um.

4.6 Development of a functional vascularized tumor melanoma spheroid

The dynamic complexity of the TME consists of different cellular components, including fibroblasts, immune cells, blood vessels, and extracellular matrix, all interacting with cancer cells to influence tumor growth and survival. This heterogeneous environment has a high impact on the response of drug treatments. In order to translate our findings to an affordable humanized melanoma model and to get further insights on the anti-tumor activity of DAC/IL-33, we generated a vascularized melanoma spheroid. To this aim, we used the OrganiX device as platform for the experimental setting (Adriani G. Pavesi A. 2024). A375M melanoma cells were labeled with PKH26 red dye and cultured via the hanging drop method for six days to allow the spheroid formation (Fig. 17A). Subsequently, each tumor spheroid was cultured in combination with GFP-expressing human umbilical vein endothelial cells (HUVEC) and normal human lung fibroblast (NHLF) at 4:1ratio, which self-assembled into a vascular network. The mixture of cells were embedded in a collagen and fibrin solution and injected into the central gel region of OrganiX to form an ECM-mimicking hydrogel. Vascularized melanoma spheroids were formed within 7 days of cell co-culture to allow the appropriate growth of the vessels network. After the complete formation of the vascularized TME (Fig. 17B), PBMCs were introduced through the side channels and exposed to the different treatment condition (DAC 0,25 μM, IL-33 100 ng/ml single or combined).

Fluorescence microscopy acquisition showed the gradual progression of vessel networks and peritumoral coverage by GFP-HUVEC fluorescence intensification around the spheroid from day 1 to day 7, i.e., prior PBMC seeding and the drug treatment (Fig. 17C). Quantitative analysis of vessel coverage through image segmentation showed increased coverage from day 1 to day 4 and no statical difference at day 7 (Fig. 17D), which can be explained with ductile endothelial

dynamics observed in response to tumor proximity. These observations demonstrate the suitability of this system for functional and molecular studies.

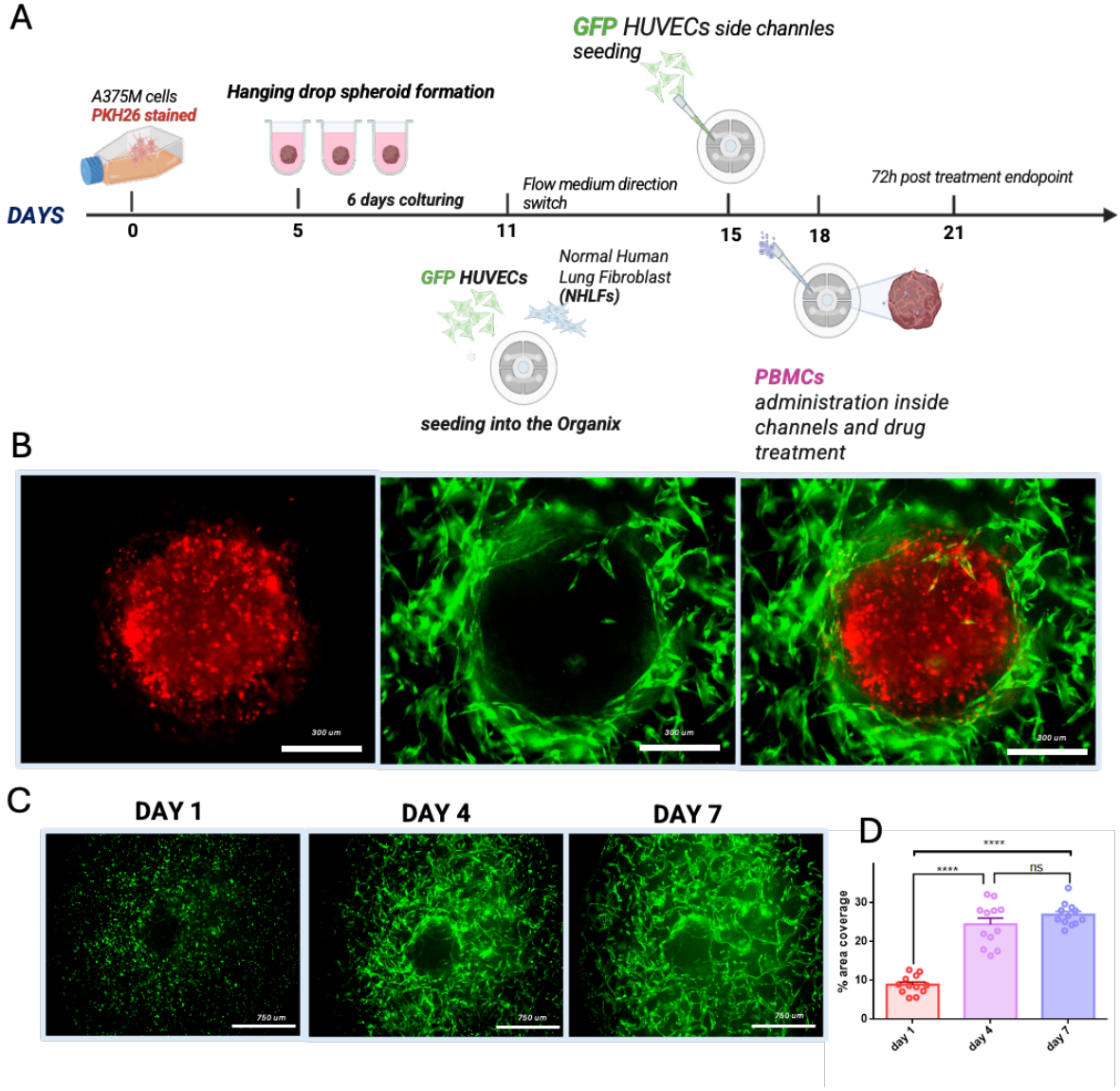

Figure 17 ***Microphysiological system with human melanoma spheroid vascularized.***

A) Schematic representation of the workflow for the 3D vascularized TME reproduction in the OrganiX system. Spheroids, HUVEC and NHLF cells were embedded with a collagen and fibrinogen mix and seeded into the main chamber, irrorated with EGM2 medium trough the side channels. NHLF supports the HUVEC endothelial cells in the formation of the vessels network allowing the perfusion of cells and drugs. B) Representative EVOS images with a 10X magnification of the tumor spheroid vascularized after 7 day of culturing. GFP HUVEC were acquired through the GFP laser and PKH26 labeled A375M cells trough the RFP. Scale bar 300 um C) Representative EVOS microphotographies of GFP HUVEC during three different time point with a 4X magnification. Scale bar 750 um D) graphical representation of coverage area (%) trough the different time points prior the drug

*treatment and PBMCs seeding (day 1, day 4 and day 7 of colture into the Organix). Statistical relevance was acquired with the one way ANOVA test and Tukey's multiple comparison test. Data represent the mean of single OrganiX devices (n=6) P value ****<0,0001 **<0,001 *<0,01*

4.7 Impact of DAC and IL-33 treatments on the vasculature phenotype

The endothelial cells form the network around the tumor and participate in promoting tumor resistance through various mechanisms (Fan J. et al. 2023). Moreover, IL-33 exhibits the ability to promote endothelial cell proliferation, migration, and morphologic differentiation, driving the assembly of expansive and highly connected vascular network (Yeon-Sook Choi et al 2009). Based on these evidence, we analyzed weather the treatments with DAC, IL-33 or their combination could impact the tumor vasculature. To this end, we isolated the HUVEC cells after culture in the OrganiX system together with melanoma spheroids and in the presence of the various treatments.

Imaging analysis showed that the vessels cultured in the presence of IL-33 alone exhibit an increased percentage of vessels area coverage compared to the untreated control and the other treatments. (Fig. 18A, B) confirming that IL-33 has a direct effect on the growth and development of the endothelial network around the tumor. IL-33 can increase vascular permeability by upregulating adhesion molecules (Laur G. et al. 2023). Mechanistically, vascular cell adhesion molecule 1 (V-CAM1) facilitates leukocyte adhesion and transmigration into tissues, serving as both a marker and mediator of a pro-inflammatory, immune-tolerant endothelium. IL-33-driven VCAM-1 expression enhances vessel permeability and network expansion, promoting immune cell recruitment (Plaques Demyanets et al 2011). Interestingly, molecular analysis of VCAM-1 shows that the endothelial cells exposed to IL-33 expressed higher levels of VCAM-1 compared to the other treatments (Fig. 18C). In contrast, addition of DAC did not enhance IL-33 induced VCAM-1 expression by HUVEC cells, suggesting that the epigenetic reprogramming does not directly affect the endothelial network.

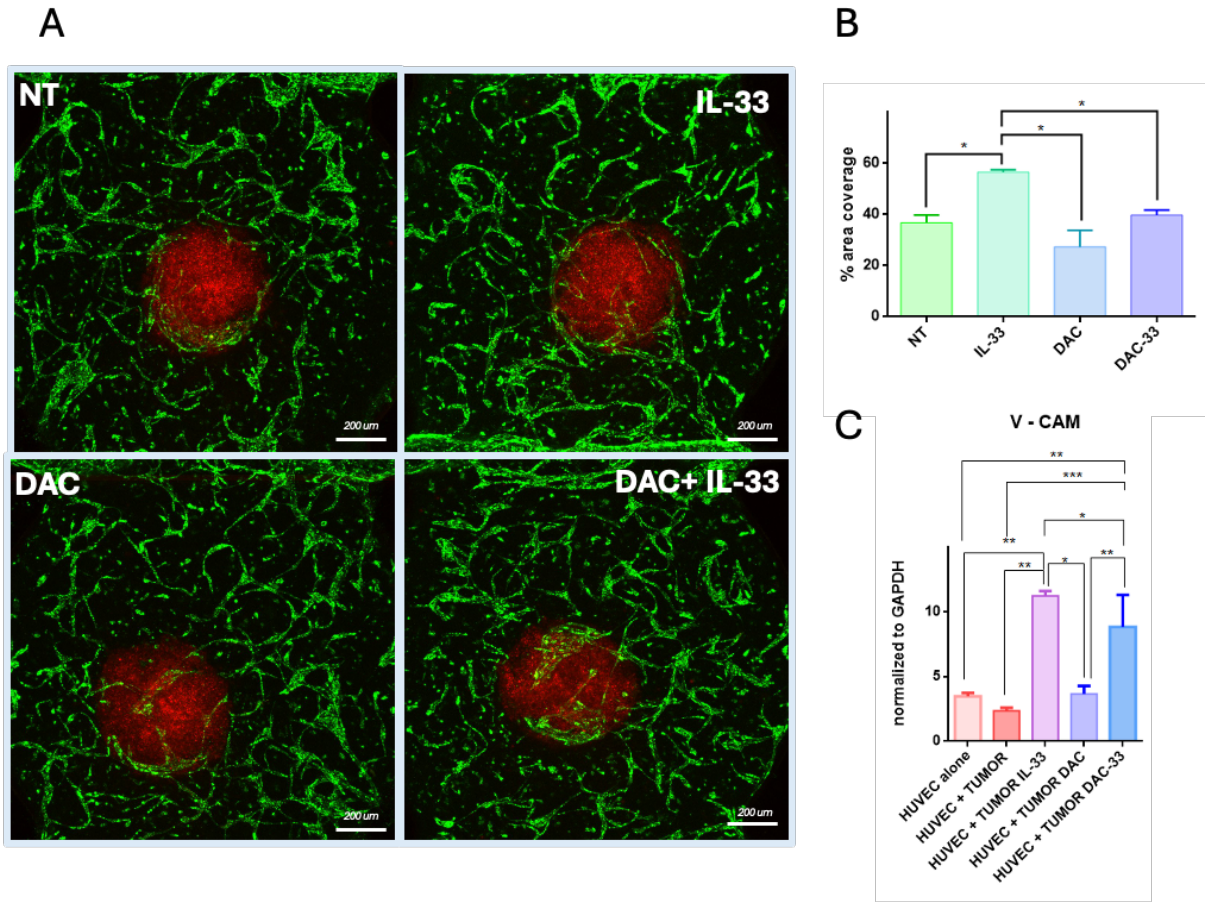

FIG 18 Effect of DAC and IL-33 treatment on the vasculature phenotype.

*A) Representative confocal acquisition with a 2,5X magnification and a 0,8 zoom of the tumor spheroid vascularized 72h post treatment with DAC, IL-33 or the combination DAC/IL-33. Scale bar 200 um B) graphical representation of coverage area (%) after 72h post treatment with DAC and IL-33 single or in combination. P value *<0.05 B) mRNA expression of V-CAM molecule normalized to GAPDH in HUVEC coltured alone, in presence of tumor and in presence of tumor with the different treatment conditions (DAC, IL-33, DAC/IL-33) Data represent the mean of single OrganiX devices (n=3) P value ****<0,0001 **<0,001 *<0,01.*

4.8 PBMCs recruitment through the vessel networks shows PD-1^{+} phenotype

Once ascertained the aptness of our vascularized melanoma model, we sought to examine the ability of drug treatments to recruit immune cells into the tumor spheroid. During the 7 days of development of the vessel network, the side channels of the OrganiX were seeded with 2x10^{5} GFP-HUVEC in 35 µl and kept in culture for three days, in order to allow the connection within the vessels inside the main chamber. PBMCs were added to the side channel of the OrganiX, in order to allow the mobility inside the vasculature, and the drug was added simultaneously to

the main chamber. Flow direction was not shifted during this co-culture time and the same volume of media was added to both sides of the devices to avoid mechanical bias for chemotactic migration of the PBMCs. Confocal images display PBMC infiltration in the microfluidic chips, revealing increased recruitment 72 h after combinatorial DAC/IL-33 treatment (Fig. 19A), which was confirmed by image based quantitative analysis of PBMC count in each tumor niche (Fig. 19B). Notably, through multicolor flow cytometry of PBMCs collected from the device we demonstrated an increment of the CD8+ PD1+ T cell population that infiltrates the tumor in presence of the DAC/IL-33 (Fig. 19C), in line with the results obtained with the *in vivo* mouse model. Overall, these findings validate our combinatory treatment into a more complex and humanized model, putting a stone for the translational relevance of this project.

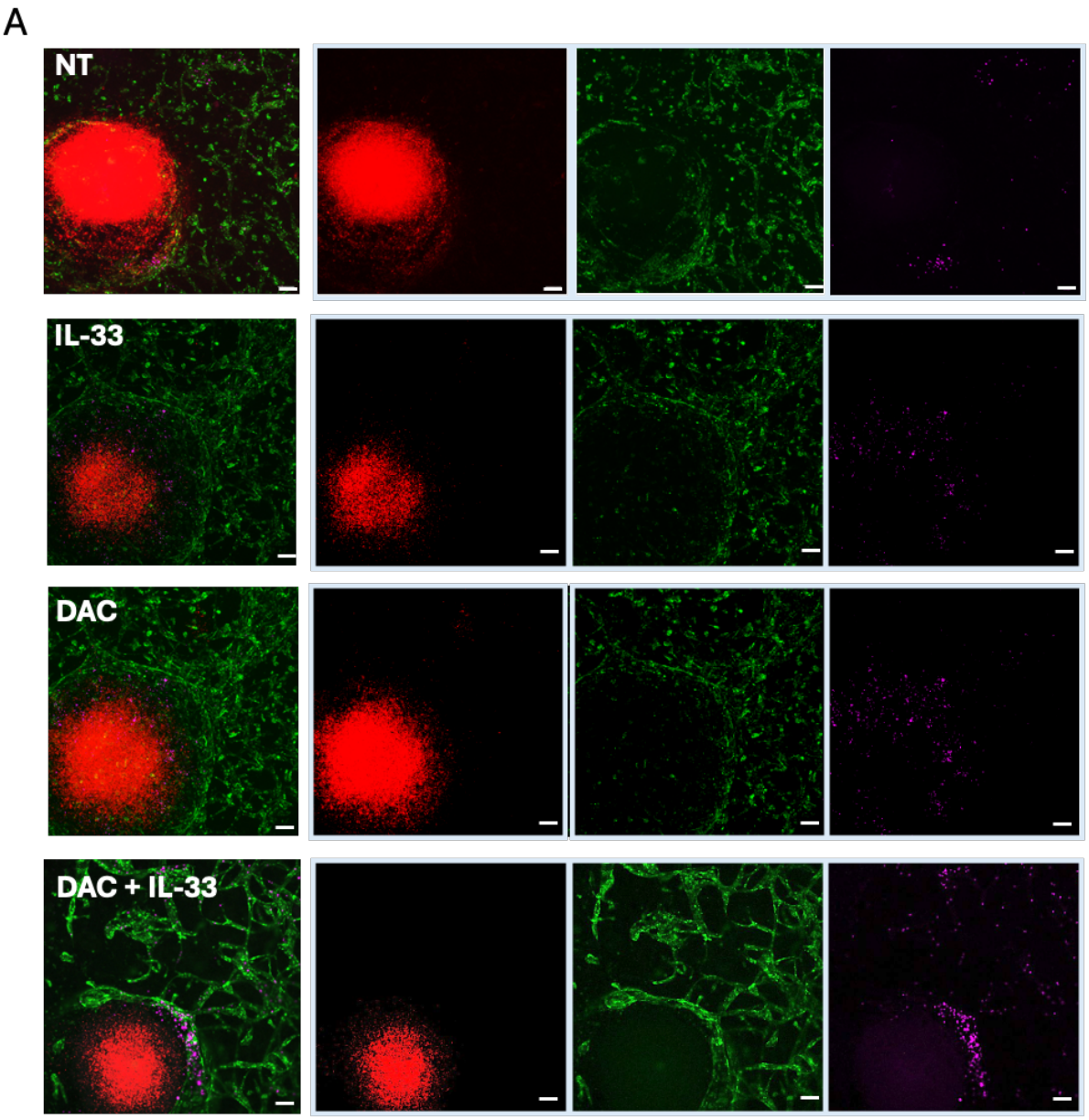
A
NT
IL-33
DAC
DAC + IL-33
PBMCs DeepRed
A375M Spheroid PKH26red
GFP-HUVEC
B
A375M
number of PBMCs infiltrate
1000
500
0
NT
IL-33
DAC
DAC-33
C
CD8+ PD1+
% CD45 live cells
15
10
5
0
NT
IL33
DAC
DAC-33

Figure* 19 *PBMCs recruitment inside the vascularized TME. *A) Max intensity Z projection and montage of confocal acquisition with a 10X magnification and a 0,5 zoom of the PMBCs (DeepRed dye labeled) infiltrating the TME through the endothelial network (GFP HUVEC) and reaching the tumor spheroid (A375M PKH26) 72h post treatment with DAC, IL-33 or the combination DAC/IL-33. Scale bar 200 um B) graphical representation of PBMCs count inside the TME for each condition after 72h post treatment with DAC and IL-33 single or in combination. (n=3) B) Flow cytometry data indicating PD1 expression on CD8+ cells 72h post treatment (DAC, IL-33, DAC/IL-33) Statistical significance across the conditions was determinate with one way ANOVA test followed by the trend analysis across treatment group. P value * < 0.05.*

4.9 DAC/IL-33 treatment improves the anti-tumor response to PD-1 blockade in vivo

Recently, the epigenetic therapy has been studied as a potential coadjutant in the overcoming of resistance to the immunotherapy with ICI (Amaro A. et al. 2023). Our *in vivo* findings underscore an increased expression of PD-1 and PD-1 expressing T cells in the TME of mice exposed to the combinatory DAC/IL-33 treatment (Fig. 5). Thus, we evaluated whether DAC/IL-33 conditioning could improve of PD-1 blockade response *in vivo*. To this aim, B16.F10 melanoma-bearing mice exposed to DAC/IL-33 combined treatment were injected with PD-1 mAb i.p. every three days starting from the last day of IL-33 injection, as illustrated in Fig. 20A.

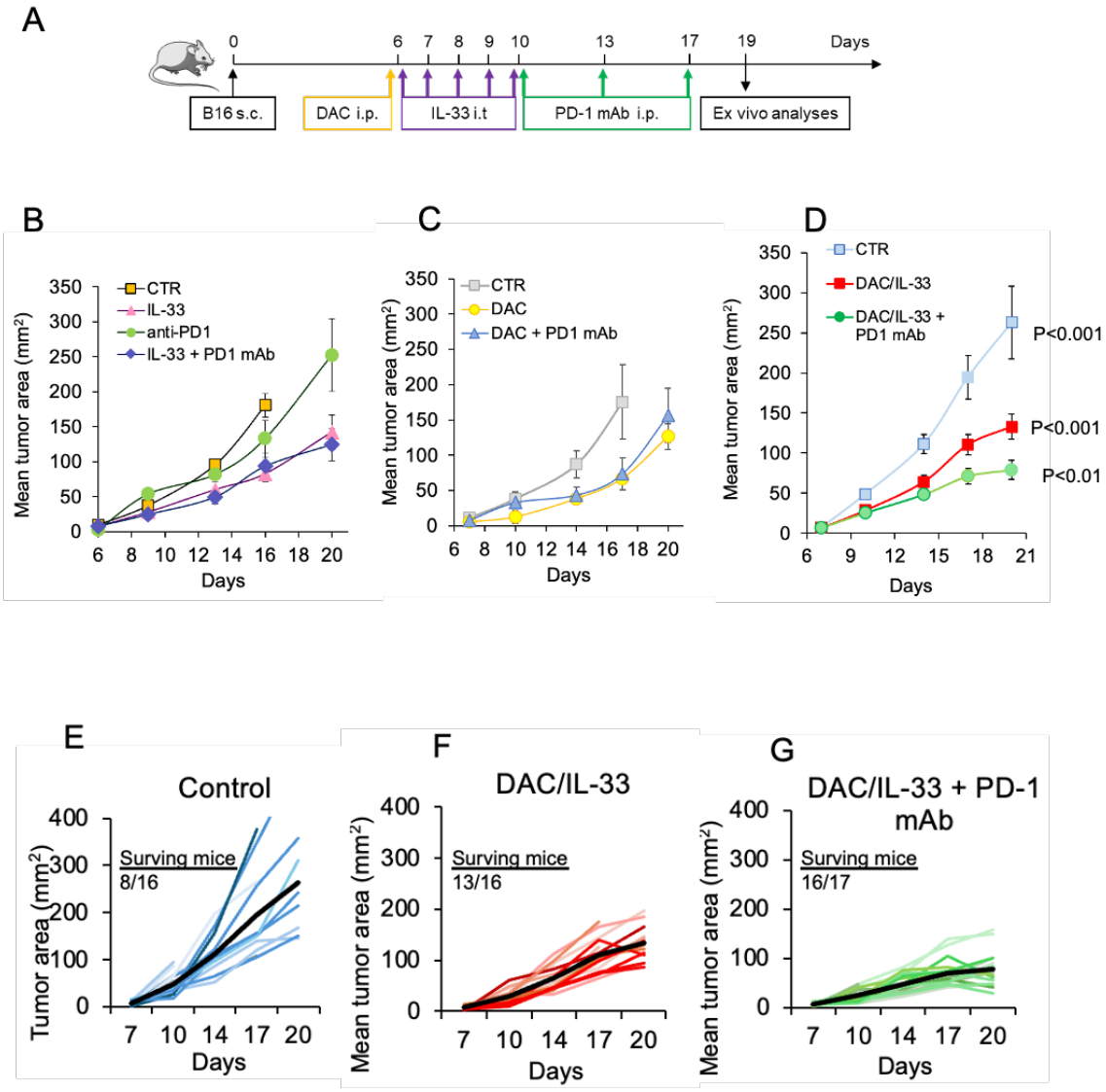

Figure 20. DAC/IL-33 treatment increases the therapeutic response to PD-1 blockade in melanoma bearing mice. *. (A) Schematic representation of experimental protocol. C57BL/6 implanted with B16.F10 melanoma cells (0.8 x 105) were treated with DAC plus IL-33 (as in Fig. 2) with or without PD-1 mAb (250 μg i.p.). Ex vivo analysis were carried out on day 19. B-D) tumor growth. B) and C) shows the effect on the tumor growth by the single DAC or IL-33 in combination (D) with the anti PD1 blockade. Mean tumor area of individual mice (n=16) ± SD. E-G) Mean tumor area of individual mice (n=16) ± SD.*

As expected, PD1 treatment failed to reduce melanoma growth, confirming that B16.F10 are unresponsive to ICI (Verma V et al 2019). Moreover, PD-1 mAb combined with either IL-33 (Fig. 20B) or DAC (Fig. 20C) had no significant impact on tumor growth reduction.

In contrast, pre-exposure to the combined DAC and IL-33 treatment unleashed the response to PD-1 blockade, as shown by significant tumor growth delay (Fig. 20D).and the improving of the survival rate (Fig. 20 E,F,G).

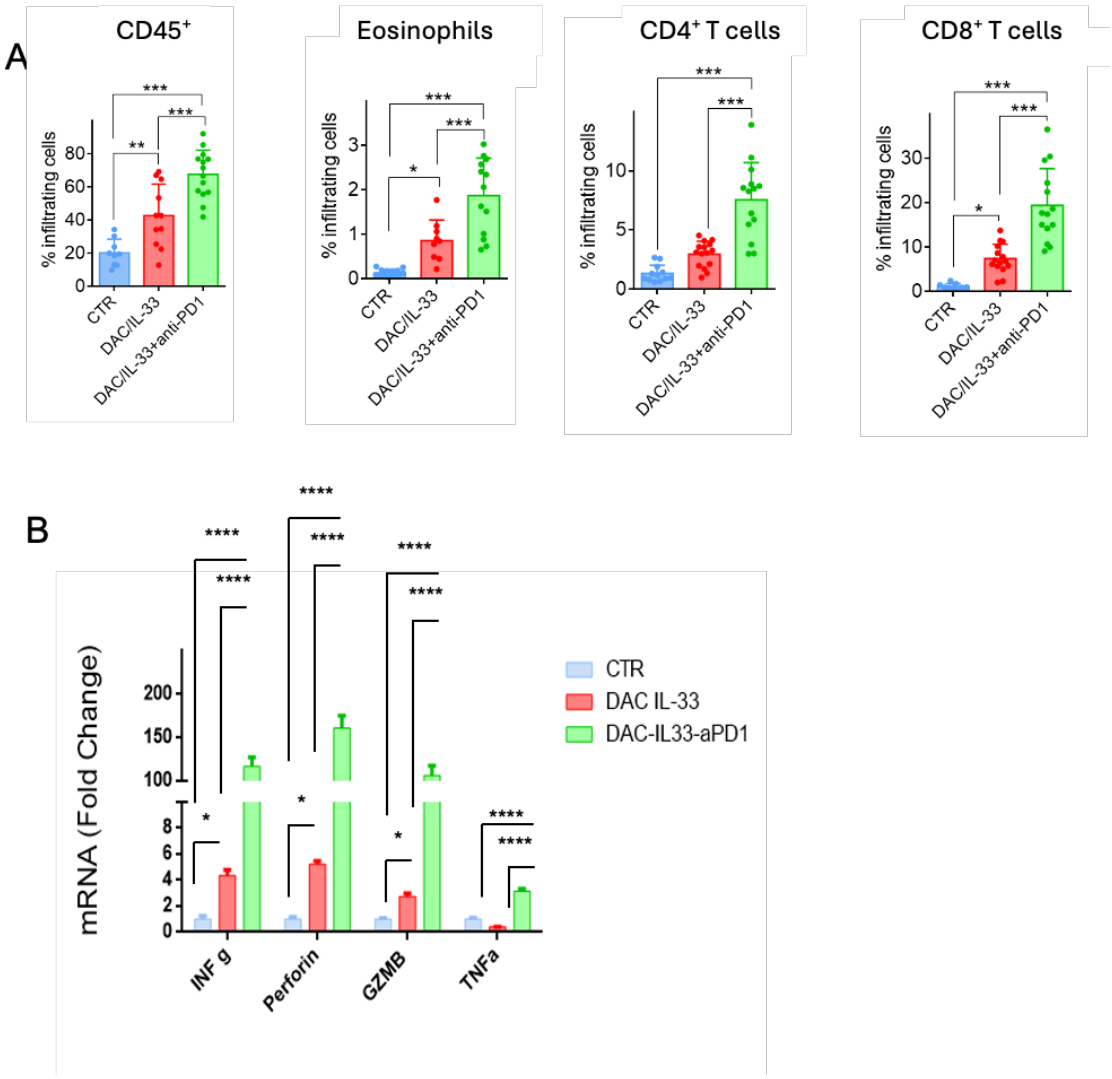

Figure 21. DAC/IL-33 treatment cooperation with PD-1 blockade in the re shaping of the TME in vivo. *A) Flow cytometry data exhibiting the major recruitment of CD45 , eosinophils CD4 and CD8 T cells . (B) Expression of indicated cytokines in melanoma tumors by real time PCR. Data are expressed as mean fold change of mRNA expression vs control of individual mice (n=7) ± SD. *P<0.05, ** P<0.01, *** P< 0.001 ****P<0.0001.*

The activation of an efficient anti-tumor response following PD-1 blockade in DAC/IL-33 treated mice was revealed by increased recruitment of CD45+ immune cells (Fig. 21A), including eosinophils, CD4+ T and CD8+ T cells and by increased intratumoral expression levels of IFN-γ, Granzyme B (GzmB), TNFα (Fig. 21B).

These data indicate that DAC plus IL-33 unleashes the therapeutic response to PD1 blockade in melanoma.

5. DISCUSSION

Melanoma is one of the most immunogenic solid tumors, exhibiting a highly mutated and neo antigen-prone nature. Its immunogenicity makes it targetable to immune checkpoint blockade-based therapies, especially PD-1 and CTLA4 inhibitors. These immunotherapies have transformed the clinical management of metastatic melanoma but still leaving a high percentage of patients facing secondary resistance to these treatments. Clinical evidence shows that the response rate for anti-PD-1 therapy alone are 30-40% that increase to a 60% after combination with CTLA-4 blockade in metastatic melanoma patients, highlighting the need for novel strategies to increase therapeutic success (Knight A. et al. 2023). Epigenetic reprogramming is a critical route to break melanoma immune resistance. Decitabine in combination with the immune-activating cytokines, such as IL-12 and IFN-I, has shown promising anti-tumor potential in preclinical models (Kozar K. 2003, Dunn & Rao, 2017). DAC not only has a direct action on the tumor cells but has been shown to increase tumor infiltrating T cells and upregulate PD-1 expression (Yu G. et al. 2019, Huang KC et al. 2020). Previous work indicates that IL-33 exerts clear anti-tumor effects in melanoma models by stimulating various immune cells such as CD8 T and NK cells (Gao X. et al. 2015, Villarreal DO. et al. 2014, Gambardella AR et al. 2024), eosinophils (Andreone S, et al. 2019 Ikutani M. et al. 2012 , Kienzl M, et al. 2020) basophils (Wagner M. et al. 2020). DC (Dominguez D. et al. 2017) and ILC2 (Kim J.et al. 2016, Payne AS. et al. 2002), thus underlining the potential of this alarmin as an immune modulator in combined therapeutic settings against melanoma.

In the present study, we demonstrate that DAC and IL-33 can synergize to remodel the TME in melanoma and result in more robust tumor control. Moreover, we show that DAC requires endogenous IL-33 signaling to promote tumor immune cell crosstalk in melanoma. In human and murine 2D and 3D spheroid models, we demonstrate the direct anti proliferative activity of DAC, but not IL-33, in line with the predominantly immunomodulatory function of this cytokine (Afferni et al. 2018). Instead, DAC displayed a combinatorial effect with IL-33 *in vivo* by remodeling the TME in mice bearing transplantable melanoma tumors. Although DAC/IL-33 did not notably inhibit tumor growth with respect to single treatments, it significantly enhanced mice survival and, most importantly, it profoundly altered the immune TME landscape. In fact, DAC/IL-33 promoted the accumulation of $CD4^+$ and $CD8^+$ T cells and strongly synergized to sustain the recruitment of eosinophils, without affecting G-MDSC. These immune traits correlated with intratumoral upregulation of Th1-related cytokines, such

as IFNγ, granzyme B and IL-12, and the chemokine CCL5, a potent chemoattractant for various immune cells, including T cells and eosinophils. Eosinophils are emerging important players in cancer immunity (Varricchi G. et al. 2018). In melanoma, IL-33-driven eosinophil recruitment and activation were shown to promote anti-tumor responses not only through indirect mechanisms (e.g., by releasing chemokines that recruit CD8+ T cells) but also through direct cytotoxicity to tumor cells (Lucarini V. et al. 2017, Carretero R. et al. 2015). Therefore, DAC/IL-33-induced immune landscape is consistent with the anti-tumorigenic activity of this combo treatment.

The greater ability of DAC/IL-33 with respect the single treatments to stimulate immune cell recruitment towards melanoma site could be confirmed by OoC experiments. These advanced models are revolutionizing the modern research, allowing specific analysis and impose new advantages into the manipulation of the TME and the possibility of a deeper understanding of the immune tumor crosstalk (Moresi et al. 2025). In competitive migration assays, mouse splenocytes migrated more vigorously towards DAC/IL-33 treated B16.F10 melanoma cells than towards untreated or single drug-treated tumor cells. Similarly, human A375M melanoma cells treated with DAC/IL-33 attracted more PBMCs, including many $CD8^+$ T cells. These findings underscore the synergistic action of DAC and IL-33 in triggering tumor-immune infiltration also in the human setting.

Another interesting finding of our study is the requirement of the IL-33/ST2 axis for the anti-tumor effectiveness of DAC *in vivo* and for driving tumor-immune recruitment. The functional need for an intact IL-33/ST2 axis for immune cell recruitment and DAC success is demonstrated by testing in ST2–/– models in which lack of ST2 is associated with both loss of therapeutic benefit and immune migration *in vivo* and in OoC assays. The early upregulation of intratumoral IL-33 and ST2 following DAC injection was associated with increased chemokines (CCL5, CCL11, CXCL9) and accumulation of CD4+, CD8+ T cells and eosinophils in TME from WT, but not $ST2^{-/-}$ mice, suggesting that intratumoral levels of IL-33 induced by DAC are required for driving immune cell recruitment. This hypothesis is corroborated by earlier work identifying IL-33–mediated control of tumor development through intra-tumoral $CD8^+$ T cell activation in PDAC and colon cancer (Moral JA, et al 2020, Xia Y, et al. 2019).

IL-33 expression is epigenetically controlled through the methylation of promoters, acetylation of histones, and repressive effects of HDAC3 in multiple pathogenic disorders (Di Salvo E, et al 2021, Zhang F. et al. 2014, Luo CH. et al. 2023). Here, we firstly show that DAC promotes IL-33 gene demethylation in solid tumors, a novel mechanism that enhances our

understanding on the regulation of this cytokine via DNA methylation. Interestingly, the observation that DAC positively modulates IL-33 and ST2 expression in the TME of melanoma-bearing mice may suggest an epigenetic control of the axis.

A notable perturbation induced by the combined DAC/IL-33 treatment in the TME of melanoma-bearing mice is the increased PD-1 expression, which occurred through a synergistic action of these drugs. This resulted in an improved response to PD-1 blockade *in vivo* highlighted by tumor growth reduction, prolonged survival and increased intratumoral immune effector cells (i.e., $CD8^+$ T, $CD4^+$ T and eosinophils) and mediators les (i.e., IFN-γ, granzyme B, perforin and TNF-α). These traits well-match a tumor reactive phenotype and indicate that DAC/IL-33 unleash the therapeutic efficacy to anti-PD-1.

In our study, neither DAC or IL-33 alone effectively ameliorated the therapeutic response to PD-1 mAb, in apparent contrast with published studies. It has been shown, in colorectal cancer (Gonda TA et al. 2020; Momparler RL. et al. 1984; Qin L, et al. 2016) and PDAC (Yue J, et al. 2024) that DAC upregulates PD-1 and PD-L1 ameliorating the effect of PD-1 blockade. In melanoma, repeated injections of DAC or its prodrug SG-110 enhanced the effect of PD-1 inhibition (Amaro A. et al. 2023). It is possible that a single injection of DAC, as we used in our study, is not sufficient to induce PD-1 (as suggested by our qPCR analysis) and, thus, to deliver therapeutic benefit for anti-PD-1 combination. IL-33 treatment in combination with PD-1 mAb was also shown to enhance the immune response in mouse model of lung cancer (Yue J, Guo et al. 2024) or prolonging the survival in mouse models of leukemia (Yue J, Guo et al. 2024) and PDAC (Moral JA, et al 2020). In our model, we injected IL-33 for five consecutive days prior to PD-1 mAb administration. This setting may be insufficient to maintain elevated levels of PD-1 throughout the mAb therapy.

The translational relevance of our findings is demonstrated by the studies in the OrganiX platform for the culture of A375M melanoma spheroids within a HUVEC-vascularized TME. Microfluidic chips supplemented with GFP-HUVECs, normal human lung fibroblasts and A375M melanoma spheroids allowed real-time longitudinal profiling of vascular network growth and architecture. Assessment by quantitative segmentation and region indicated that vessel coverage improved from the first day through day 7, demonstrating dynamic and adaptive remodeling in response to tumor-derived signals and cytokine/epigenetic signals. These findings align with existing models suggesting that vessel normalization and activation are critical prerequisites for immune cell infiltration and enhanced immunotherapy efficacy (Carretero R. et al 2015). On a molecular level, analysis of the effect of DAC and IL-33, alone or combined, showed significantly increased expression of VCAM-1, a high endothelial

activation marker and leukocyte recruitment facilitator (Kaur, G. 2023) Interestingly, IL-33 alone had the strongest effect in the activation of VCAM-1. These finding well correlates with previous studies showing IL-33 to be activator of VCAM-1 and consequentially an indirect agent of angiogenesis (Demyanets S, et al. 2011, Demyanets S. et al. 2021). In contrast, DAC is known to interfere with neo angiogenesis by affecting the release of MMP9 and MMP2 in a gastric carcinoma study (Shin DY, et al. 2012). This may explain the lower expression of VCAM-1 by the HUVEC exposed to the combinational therapy.

Nevertheless, in our vascularized melanoma model we confirmed the superior ability of the DAC (IL-33 combination to recruit immune cells (i.e., PBMCs) in the TME. Notably, we found increased PD-1 expression in the CD8 infiltrating the tumor. Recent studies have linked the response to ICI to PD-1^{+}TCF-1^{+} stem-like rather than terminally exhausted $CD8^{+}$ T cells. (Miller, B.C., et al. 2019). In murine models, tumor-associated high endothelial venule ECs (TA-HECs) derived from post-capillary venules are recruited into tumors and associated with different types of T cells. Enhancement of TA-HECs leads to higher proportions of anti-tumor stem-like CD8+ T cells and improves the effectiveness of ICI (Asrir A, et al. 2022). The ensemble of these findings may suggest that DAC/IL-33 can have a double action on the TME by promoting the immune recruitment and activation and by stimulating the development of TA HECs, leading to anti-tumor stem like CD8 population to possible enhance the anti PD-1 effect. In conclusion, our study unravels the importance of IL-33/ST2 axis in driving the immune crosstalk and indicate DAC as a positive regulator of the axis that can further increase the effect of IL-33 against melanoma including ICI. Vascularized tumor models have provided a direct demonstration of the ability of combined DAC/IL-33 treatment to enhance the infiltration of PBMCs, and molecular analyses confirm that PD-1 expression increases in infiltrating $CD8^{+}$ T cells. Additionally, IL-33-induced VCAM-1 activation, which contributes directly to immune cell adhesion and functions in angiogenesis, sheds new light on endothelial plasticity within the TME. Together, our results enhance our understanding of the mechanistic basis of melanoma immune resistance as well as help characterize implementable axes of intervention.

6. REFERENCES

1. A. Hunter Shai, Iwei Yeh, Ivanka Kovalyshyn, Aravindhan Sriharan, Eric Talevic ,Alexander Gagnon, Reinhard Dummer, Jeffrey North, Laura Pincus, Beth Ruben, William

Rickaby ,Corrado D'Arrigo, Alistair Robson ,Boris C. Bastian: The Genetic Evolution of Melanoma from Precursor Lesions 2015 New England Journal of Medicine 1926-1936 ,Vol 373 , n 20, 2015 doi:10.1056/NEJMoa1502583EJMoa1502583
2. Adriani, G., Pavesi, A. The OrganiX microfluidic system to recreate the complex tumour microenvironment. *Nat Rev Immunol* **24**, 307 (2024). https://doi.org/10.1038/s41577-024-01011-x
3. Afferni C, Buccione C, Andreone S, Galdiero MR, Varricchi G, Marone G, Mattei F, Schiavoni G. The Pleiotropic Immunomodulatory Functions of IL-33 and Its Implications in Tumor Immunity. Front Immunol. 2018 Nov 13;9:2601. doi: 10.3389/fimmu.2018.02601. PMID: 30483263; PMCID: PMC6242976
4. Akimoto M, Maruyama R, Takamaru H, Ochiya T, Takenaga K. Soluble IL-33 receptor sST2 inhibits colorectal cancer malignant growth by modifying the tumour microenvironment. Nat Commun. 2016 Nov 24;7:13589. doi: 10.1038/ncomms13589. PMID: 27882929; PMCID: PMC5123057
5. Ali, S., Nguyen, D. Q., Falk, W. & Martin, M. U. Caspase 3 inactivates biologically active full length interleukin-33 as a classical cytokine but does not prohibit nuclear translocation. *Biochem Biophys Res Commun* **391**, 1512–1516, https://doi.org/10.1016/j.bbrc.2009.12.107 (2010).
6. Amaro A, Reggiani F, Fenoglio D, Gangemi R, Tosi A, Parodi A, Banelli B, Rigo V, Mastracci L, Grillo F, Cereghetti A, Tastanova A, Ghosh A, Sallustio F, Emionite L, Daga A, Altosole T, Filaci G, Rosato A, Levesque M, Maio M, Pfeffer U, Croce M; EPigenetic Immune-oncology Consortium Airc (EPICA) consortium. Guadecitabine increases response to combined anti-CTLA-4 and anti-PD-1 treatment in mouse melanoma in vivo by controlling T-cells, myeloid derived suppressor and NK cells. J Exp Clin Cancer Res. 2023 Mar 18;42(1):67. doi: 10.1186/s13046-023-02628-x. PMID: 36934257; PMCID: PMC10024396.
7. Amisaki, M., Zebboudj, A., Yano, H. *et al.* IL-33-activated ILC2s induce tertiary lymphoid structures in pancreatic cancer. *Nature* **638**, 1076–1084 (2025). https://doi.org/10.038/s41586-024-08426-5
8. Andreone S, Gambardella AR, Mancini J, Loffredo S, Marcella S, La Sorsa V, et al. Anti-Tumorigenic Activities of IL-33: A Mechanistic Insight. Front Immunol. 2020;11:571593. doi: 10.3389/fimmu.2020.571593.
9. Andreone S, Spadaro F, Buccione C, Mancini J, Tinari A, Sestili P, et al. IL-33 Promotes CD11b/CD18-Mediated Adhesion of Eosinophils to Cancer Cells and Synapse-Polarized Degranulation Leading to Tumor Cell Killing. Cancers (Basel). 2019;11(11). doi: 10.3390/cancers11111664
10. Blomberg OS, Spagnuolo L, Garner H, Voorwerk L, Isaeva OI, van Dyk E, et al. IL-5-producing CD4+ T cells and eosinophils cooperate to enhance response to immune checkpoint blockade in breast cancer. Cancer Cell. 2023;41(1):106-23.e10. doi: 10.1016/j.ccell.2022.11.014.
11. Bomar L, Senithilnathan A, Ahn C. Systemic Therapies for Advanced Melanoma. Dermatol Clin. 2019 Oct;37(4):409-423. doi: 10.1016/j.det.2019.05.001. Epub 2019 Jul 10. PMID: 31466582.
12. Businaro L, De Ninno A, Schiavoni G, Lucarini V, Ciasca G, Gerardino A, Belardelli F, Gabriele L, Mattei F. Cross talk between cancer and immune cells: exploring complex dynamics in a microfluidic environment. Lab Chip. 2013 Jan 21;13(2):229-39. doi: 10.1039/c2lc40887b. Epub 2012 Oct 30. PMID: 23108434.
13. Candido S, Rapisarda V, Marconi A, Malaponte G, Bevelacqua V, Gangemi P, Scalisi A, McCubrey JA, Maestro R, Spandidos DA, Spandidos DA, et al: Analysis of the B-

RafV600E mutation in cutaneous melanoma patients with occupational sun exposure. Oncol Rep 31: 1079-1082, 2014.
14. Carreira S, Goodall J, Aksan I, La Rocca SA, Galibert MD, Denat L, Larue L, Goding CR. Mitf cooperates with Rb1 and activates p21Cip1 expression to regulate cell cycle progression. Nature. 2005 Feb 17;433(7027):764-9. doi: 10.1038/nature03269. PMID: 15716956.
15. Carreira S, Goodall J, Denat L, Rodriguez M, Nuciforo P, Hoek KS, Testori A, Larue L, Goding CR. Mitf regulation of Dia1 controls melanoma proliferation and invasiveness. Genes Dev. 2006 Dec 15;20(24):3426-39. doi: 10.1101/gad.406406. PMID: 17182868; PMCID: PMC1698449.
16. Carretero R, Sektioglu IM, Garbi N, Salgado OC, Beckhove P, Hämmerling GJ. Eosinophils orchestrate cancer rejection by normalizing tumor vessels and enhancing infiltration of CD8(+) T cells. Nat Immunol. 2015;16(6):609-17. doi: 10.1038/ni.3159.
17. Carriere, V. *et al*. IL-33, the IL-1-like cytokine ligand for ST2 receptor, is a chromatin-associated nuclear factor *in vivo*. *Proc Natl Acad Sci USA* **104**, 282–287, https://doi.org/10.1073/pnas.0606854104 (2007).
18. Cataldo, V. D., Cortes, J., & Quintás-Cardama, A. (2009). Azacitidine for the treatment of myelodysplastic syndrome. *Expert Review of Anticancer Therapy*, *9*(7), 875–884. https://doi.org/10.1586/era.09.61
19. Cayrol C, Duval A, Schmitt P, Roga S, Camus M, Stella A, et al. Environmental allergens induce allergic inflammation through proteolytic maturation of IL-33. *Nat Immunol.* (2018) 19:375–85. doi: 10.1038/s41590-018-0067-5
20. Cayrol C, Girard J-P. Interleukin-33 (IL-33): a nuclear cytokine from the IL-1 family. *Immunol Rev.* (2018) 281:154–68. doi: 10.1111/imr.12619
21. Chen L, Sun R, Xu J, Zhai W, Zhang D, Yang M, et al. Tumor-Derived IL33 Promotes Tissue-Resident CD8+ T Cells and Is Required for Checkpoint Blockade Tumor Immunotherapy. Cancer Immunol Res. 2020;8(11):1381-92. doi: 10.1158/2326-6066.CIR-19-1024.
22. Choubey D. Type I interferon (IFN)-inducible Absent in Melanoma 2 proteins in neuroinflammation: implications for Alzheimer's disease. J Neuroinflammation. 2019 Nov 26;16(1):236. doi: 10.1186/s12974-019-1639-5. PMID: 31771614; PMCID: PMC6880379.
23. Coventry BJ. Therapeutic vaccination immunomodulation: forming the basis of all cancer immunotherapy. Ther Adv Vaccines Immunother. 2019 Aug 1;7:2515135519862234. doi: 10.1177/2515135519862234. PMID: 31414074; PMCID: PMC6676259.
24. Daniel O. Villarreal, Megan C. Wise, Jewell N. Walters, Emma L. Reuschel, Min Joung Choi, Nyamekye Obeng-Adjei, Jian Yan, Matthew P. Morrow, David B. Weiner; Alarmin IL-33 Acts as an Immunoadjuvant to Enhance Antigen-Specific Tumor Immunity. *Cancer Res* 15 March 2014; 74 (6): 1789–1800. https://doi.org/10.1158/0008-5472.CAN-13-2729
25. Daskalakis M, Blagitko-Dorfs N, Hackanson B. Decitabine. Recent Results Cancer Res. 2010;184:131-57. doi: 10.1007/978-3-642-01222-8_10. PMID: 20072836.
26. de la Serna Ivana L., Ohkawa Yasuyuki, Higashi Chiduru, Dutta Chaitali, Osias Jules, Kommajosyula Naveen, Tachibana Taro, Imbalzano Anthony N. The Microphthalmia-associated Transcription Factor Requires SWI/SNF Enzymes to Activate Melanocyte-specific Genes (2006) Journal of Biological Chemistry, Volume 281, Issue 29, 20233 – 20241 doi: 10.1074/jbc.M512052200
27. Demyanets S, Stojkovic S, Huber K, Wojta J. The Paradigm Change of IL-33 in Vascular Biology. Int J Mol Sci. 2021 Dec 10;22(24):13288. doi: 10.3390/ijms222413288. PMID: 34948083; PMCID: PMC8707059.
28. Demyanets Svitlana, KonyaViktoria, Kastl Stefan P., Kaun Christoph, Rauscher Sabine, Niessner Alexander, Pentz Richard, Pfaffenberger Stefan, Rychl, Kathrin, Lemberger

Christof E., de Martin Rainer, Heinemann Akos, Huk Ihor, Gröger Marion, Maurer Gerald, Huber Kurt, Wojta Johann Interleukin-33 Induces Expression of Adhesion Molecules and Inflammatory Activation in Human Endothelial Cells and in Human Atherosclerotic, Arteriosclerosis, Thrombosis, and Vascular Biology 2011 2011/09/01 doi: 10.1161/ATVBAHA.111.231431
29. Di Salvo E, Casciaro M, Gangemi S. IL-33 genetics and epigenetics in immune-related diseases. Clin Mol Allergy. 2021;19(1):18. doi: 10.1186/s12948-021-00157-6.
30. Dinarello, Charles A. Overview of the IL-1 family in innate inflammation and acquired immunity, Immunological Reviews Volume 281 ISSN 10105-2896 https://doi.org/10.1111/imr.12621
31. Dixit A, Sarver A, Zettervall J, Huang H, Zheng K, Brekken RA, et al. Targeting TNF-α-producing macrophages activates antitumor immunity in pancreatic cancer via IL-33 signaling. JCI Insight. 2022;7(22). doi: 10.1172/jci.insight.153242.
32. Dominguez D, Ye C, Geng Z, Chen S, Fan J, Qin L, et al. Exogenous IL-33 Restores Dendritic Cell Activation and Maturation in Established Cancer. J Immunol. 2017;198(3):1365-75. doi: 10.4049/jimmunol.1501399.
33. Espen S. Baekkevold, Myriam Roussigné, Takeshi Yamanaka, Finn-Eirik Johansen, Frode L. Jahnsen, François Amalric, Per Brandtzaeg, Monique Erard, Guttorm Haraldsen, Jean-Philippe Girard, Molecular Characterization of NF-HEV, a Nuclear Factor Preferentially Expressed in Human High Endothelial Venules,The American Journal of Pathology, Volume 163, Issue 1,2003,Pages 69-79,ISSN 0002-9440 https://doi.org/10.1016/S0002-9440(10)63631-0 .
34. F. Moresi, F. Noto, J. Vasudevan, X. Bisteau, G. Adriani, and A. Pavesi, " Microphysiological Systems in Cancer Research: Advancing Immunotherapy through Tumor Microenvironment-Integrated Organ-On-Chip Models." *Adv. Therap.* 8, no. 9 (2025): 8, e00098. **https://doi.org/10.1002/adtp.202500098**
35. Fang, J., Lu, Y., Zheng, J. *et al.* Exploring the crosstalk between endothelial cells, immune cells, and immune checkpoints in the tumor microenvironment: new insights and therapeutic implications. *Cell Death Dis* **14**, 586 (2023). https://doi.org/10.1038/s41419-023-06119-x
36. Fournié Jean-Jacques , Poupot Mary The Pro-tumorigenic IL-33 Involved in Antitumor Immunity: A Yin and Yang Cytokine Frontiers in Immunology Volume 9 - 2018
37. Gao X, Wang X, Yang Q, Zhao X, Wen W, Li G, et al. Tumoral expression of IL-33 inhibits tumor growth and modifies the tumor microenvironment through CD8+ T and NK cells. J Immunol. 2015;194(1):438-45. doi: 10.4049/jimmunol.140134
38. Gillibert-Duplantier J, Duthey B, Sisirak V, Salaün D, Gargi T, Trédan O, Finetti P, Bertucci F, Birnbaum D, Bendriss-Vermare N, Badache A. Gene expression profiling identifies sST2 as an effector of ErbB2-driven breast carcinoma cell motility, associated with metastasis. Oncogene. 2012 Jul 26;31(30):3516-24. doi: 10.1038/onc.2011.525. Epub 2011 Nov 21. PMID: 22105364.
39. Giunta EF, Arrichiello G, Curvietto M, Pappalardo A, Bosso D, Rosanova M, Diana A, Giordano P, Petrillo A, Federico P, Fabozzi T, Parola S, Riccio V, Mucci B, Vanella V, Festino L, Daniele B, Ascierto PA, Ottaviano M, On Behalf Of Scito Youth. Epigenetic Regulation in Melanoma: Facts and Hopes. Cells. 2021 Aug 11;10(8):2048. doi: 10.3390/cells10082048. PMID: 34440824; PMCID: PMC8392422.
40. Gordy JT, Luo K, Kapoor A, Kim ES, Ayeh SK, Karakousis PC, et al. Treatment with an immature dendritic cell-targeting vaccine supplemented with IFN-α and an inhibitor of DNA methylation markedly enhances survival in a murine melanoma model. Cancer Immunol Immunother. 2020;69(4):569-80. doi: 10.1007/s00262-019-02471-0.

41. Gordy JT, Sandhu AK, Fessler K, Luo K, Kapoor AR, Ayeh SK, et al. IFNα and 5-Aza-2'-deoxycytidine combined with a dendritic-cell targeting DNA vaccine alter tumor immune cell infiltration in the B16F10 melanoma model. Front Immunol. 2022;13:1074644. doi: 10.3389/fimmu.2022.1074644.
42. Gracia-Hernandez M, Munoz Z, Villagra A. Enhancing Therapeutic Approaches for Melanoma Patients Targeting Epigenetic Modifiers. Cancers (Basel). 2021 Dec 8;13(24):6180. doi: 10.3390/cancers13246180. PMID: 34944799; PMCID: PMC8699560.
43. Han J, Xu X, Liu Z, Li Z, Wu Y, Zuo D. Recent advances of molecular mechanisms of regulating PD-L1 expression in melanoma. Int Immunopharmacol. 2020;88:106971. doi: 10.1016/j.intimp.2020.106971.
44. Hollande C, Boussier J, Ziai J, Nozawa T, Bondet V, Phung W, Lu B, Duffy D, Paradis V, Mallet V, Eberl G, Sandoval W, Schartner JM, Pol S, Barreira da Silva R, Albert ML. Inhibition of the dipeptidyl peptidase DPP4 (CD26) reveals IL-33-dependent eosinophil-mediated control of tumor growth. Nat Immunol. 2019 Mar;20(3):257-264. doi: 10.1038/s41590-019-0321-5. Epub 2019 Feb 18. PMID: 30778250.
45. Huang KC, Chiang SF, Chen WT, Chen TW, Hu CH, Yang PC, et al. Decitabine Augments Chemotherapy-Induced PD-L1 Upregulation for PD-L1 Blockade in Colorectal Cancer. Cancers (Basel). 2020;12(2). doi: 10.3390/cancers12020462.
46. Ikutani M, Yanagibashi T, Ogasawara M, Tsuneyama K, Yamamoto S, Hattori Y, et al. Identification of innate IL-5-producing cells and their role in lung eosinophil regulation and antitumor immunity. J Immunol. 2012;188(2):703-13. doi: 10.4049/jimmunol.1101270.
47. Jabbour E, Issa JP, Garcia-Manero G, Kantarjian H. Evolution of decitabine development: accomplishments, ongoing investigations, and future strategies. Cancer. 2008 Jun;112(11):2341-51. doi: 10.1002/cncr.23463. PMID: 18398832; PMCID: PMC4784235.
48. Jacquelot N, Seillet C, Wang M, Pizzolla A, Liao Y, Hediyeh-Zadeh S, Grisaru-Tal S, Louis C, Huang Q, Schreuder J, Souza-Fonseca-Guimaraes F, de Graaf CA, Thia K, Macdonald S, Camilleri M, Luong K, Zhang S, Chopin M, Molden-Hauer T, Nutt SL, Umansky V, Ciric B, Groom JR, Foster PS, Hansbro PM, McKenzie ANJ, Gray DHD, Behren A, Cebon J, Vivier E, Wicks IP, Trapani JA, Munitz A, Davis MJ, Shi W, Neeson PJ, Belz GT. Blockade of the co-inhibitory molecule PD-1 unleashes ILC2-dependent antitumor immunity in melanoma. Nat Immunol. 2021 Jul;22(7):851-864. doi: 10.1038/s41590-021-00943-z. Epub 2021 Jun 7. PMID: 34099918; PMCID: PMC7611091.
49. Jovanovic I, Radosavljevic G, Mitrovic M, Juranic VL, McKenzie AN, Arsenijevic N, Jonjic S, Lukic ML. ST2 deletion enhances innate and acquired immunity to murine mammary carcinoma. Eur J Immunol. 2011 Jul;41(7):1902-12. doi: 10.1002/eji.201141417. PMID: 21484786; PMCID: PMC3746127.
50. Kaur, G., Sharma, D., Bisen, S. *et al.* Vascular cell-adhesion molecule 1 (VCAM-1) regulates JunB-mediated IL-8/CXCL1 expression and pathological neovascularization. *Commun Biol* **6**, 516 (2023). https://doi.org/10.1038/s42003-023-04905-z
51. Kienzl M, Hasenoehrl C, Valadez-Cosmes P, Maitz K, Sarsembayeva A, Sturm E, et al. IL-33 reduces tumor growth in models of colorectal cancer with the help of eosinophils. Oncoimmunology. 2020;9(1). doi: 10.1080/2162402X.2020.1776059.
52. Kim J, Kim W, Moon UJ, Kim HJ, Choi HJ, Sin JI, et al. Intratumorally Establishing Type 2 Innate Lymphoid Cells Blocks Tumor Growth. J Immunol. 2016;196(5):2410-23. doi: 10.4049/jimmunol.1501730.
53. Knight, A.; Karapetyan, L.; Kirkwood, J.M. Immunotherapy in Melanoma: Recent Advances and Future Directions. *Cancers* **2023**, *15*, 1106. https://doi.org/10.3390/cancers15041106

54. Kostaki, M., Manona, A.D., Stavraka, I., Korkolopoulou, P., Levidou, G., Trigka, E.-A., Christofidou, E., Champsas, G., Stratigos, A.J., Katsambas, A., Papadopoulos, O., Piperi, C. and Papavassiliou, A.G. (2014), High-frequency *p16^{INK4A}* promoter methylation is associated with histone methyltransferase SETDB1 expression in sporadic cutaneous melanoma. Exp Dermatol, 23: 332-338. https://doi.org/10.1111/exd.12398
55. Kozar K, Kamiński R, Switaj T, Ołdak T, Machaj E, Wysocki PJ, Mackiewicz A, Lasek W, Jakóbisiak M, Gołab J. Interleukin 12-based immunotherapy improves the antitumor effectiveness of a low-dose 5-Aza-2'-deoxycitidine treatment in L1210 leukemia and B16F10 melanoma models in mice. Clin Cancer Res. 2003 Aug 1;9(8):3124-33. PMID: 12912964.
56. Lahtz C., Stranzenbach R., Fiedler E., Helmbold P., Dammann R.H. Methylation of PTEN as a Prognostic Factor in Malignant Melanoma of the Skin. J. Investig. Dermatol. 2010;130:620–622. doi: 10.1038/jid.2009.226.
57. Lam M, Reales-Calderon JA, Ow JR, Adriani G, Pavesi A. *In vitro* 3D liver tumor microenvironment models for immune cell therapy optimization. APL Bioeng. 2021 Oct 4;5(4):041502. doi: 10.1063/5.0057773. PMID: 34632251; PMCID: PMC8492081.
58. Larsen KM, Minaya MK, Vaish V, Peña MMO. The Role of IL-33/ST2 Pathway in Tumorigenesis. Int J Mol Sci. 2018 Sep 9;19(9):2676. doi: 10.3390/ijms19092676. PMID: 30205617; PMCID: PMC6164146.
59. Lauss M., Haq R., Cirenajwis H., Phung B., Harbst K., Staaf J., Rosengren F., Holm K., Aine M., Jirström K., et al. Genome-Wide DNA Methylation Analysis in Melanoma Reveals the Importance of CpG Methylation in MITF Regulation. J. Investig. Dermatol. 2015;135:1820–1828. doi: 10.1038/jid.2015.61
60. Lefrançais E, Duval A, Mirey E, Roga S, Espinosa E, Cayrol C, et al. Central domain of IL-33 is cleaved by mast cell proteases for potent activation of group-2 innate lymphoid cells. *Proc Natl Acad Sci USA.* (2014) 111:15502–7. doi: 10.1073/pnas.1410700111
61. Lefrançais E, Roga S, Gautier V, Gonzalez-de-Peredo A, Monsarrat B, Girard JP, Cayrol C. IL-33 is processed into mature bioactive forms by neutrophil elastase and cathepsin G. Proc Natl Acad Sci U S A. 2012 Jan 31;109(5):1673-8. doi: 10.1073/pnas.1115884109. Epub 2012 Jan 17. PMID: 22307629; PMCID: PMC3277172.
62. Leiter U., Schmid R.M., Kaskel P., Peter R.U., Krähn G. Antiapoptotic Bcl-2 and Bcl-XL in Advanced Malignant Melanoma. Arch. Dermatol. Res. 2000;292:225–232. doi: 10.1007/s004030050479
63. Li X, Li Y, Dong L, Chang Y, Zhang X, Wang C, Chen M, Bo X, Chen H, Han W, Nie J. Decitabine priming increases anti-PD-1 antitumor efficacy by promoting CD8+ progenitor exhausted T cell expansion in tumor models. J Clin Invest. 2023 Apr 3;133(7):e165673. doi: 10.1172/JCI165673. PMID: 36853831; PMCID: PMC10065084.
64. Liew, F., Girard, JP. & Turnquist, H. Interleukin-33 in health and disease. *Nat Rev Immunol* **16**, 676–689 (2016). https://doi.org/10.1038/nri.2016.95
65. Loercher AE, Tank EM, Delston RB, Harbour JW. MITF links differentiation with cell cycle arrest in melanocytes by transcriptional activation of INK4A. J Cell Biol. 2005 Jan 3;168(1):35-40. doi: 10.1083/jcb.200410115. Epub 2004 Dec 28. PMID: 15623583; PMCID: PMC2171666.
66. Lucarini V, Buccione C, Zicchedda G, Peschiaroli F, Sestili P, Puglisi R, et al. Combining Type I Interferons and 5-Aza-2?-Deoxycitidine to Improve Anti-Tumor Response against Melanoma. Journal of Investigative Dermatology. 2017;137(1):159-69. doi: 10.1016/j.jid.2016.08.024.
67. Luo CH, Lai AC, Chang YJ. Butyrate inhibits Staphylococcus aureus-aggravated dermal IL-33 expression and skin inflammation through histone deacetylase inhibition. Front Immunol. 2023;14:1114699. doi: 10.3389/fimmu.2023.1114699.

68. M. Raza Zaidi, Chi-Ping Day, Glenn Merlino,From UVs to Metastases: Modeling Melanoma Initiation and Progression in the Mouse,Journal of Investigative DermatologyVolume 128, Issue 10,2008,Pages 2381-2391,ISSN 0022-202X,https://doi.org/10.1038/jid.2008.177.
69. Mattei F, Andreone S, Mencattini A, De Ninno A, Businaro L, Martinelli E, Schiavoni G. Oncoimmunology Meets Organs-on-Chip. Front Mol Biosci. 2021 Mar 26;8:627454. doi: 10.3389/fmolb.2021.627454. PMID: 33842539; PMCID: PMC8032996.
70. Miller, B.C., Sen, D.R., Al Abosy, R. *et al.* Subsets of exhausted $CD8^+$ T cells differentially mediate tumor control and respond to checkpoint blockade. *Nat Immunol* **20**, 326–336 (2019). https://doi.org/10.1038/s41590-019-0312-6
71. Momparler RL, Samson J, Momparler LF, Rivard GE. Cell cycle effects and cellular pharmacology of 5-aza-2'-deoxycytidine. Cancer Chemother Pharmacol. 1984;13(3):191-4. doi: 10.1007/BF00269027.
72. Moral JA, Leung J, Rojas LA, Ruan J, Zhao J, Sethna Z, et al. ILC2s amplify PD-1 blockade by activating tissue-specific cancer immunity. Nature. 2020. doi: 10.1038/s41586-020-2015-4.
73. Moral JA, Leung J, Rojas LA, Ruan J, Zhao J, Sethna Z, Ramnarain A, Gasmi B, Gururajan M, Redmond D, Askan G, Bhanot U, Elyada E, Park Y, Tuveson DA, Gönen M, Leach SD, Wolchok JD, DeMatteo RP, Merghoub T, Balachandran VP. ILC2s amplify PD-1 blockade by activating tissue-specific cancer immunity. Nature. 2020 Mar;579(7797):130-135. doi: 10.1038/s41586-020-2015-4. Epub 2020 Feb 19. PMID: 32076273; PMCID: PMC7060130.
74. Mousa Komai-Koma, Eryi Wang, Mariola Kurowska-Stolarska, Dong Li, Charles McSharry, Damo Xu,Interleukin-33 promoting Th1 lymphocyte differentiation dependents on IL-12, Immunobiology, Volume 221, Issue 3, 2016,Pages 412-417,ISSN 0171-2985,https://doi.org/10.1016/j.imbio.2015.11.013.
75. Mousa Komai-Koma, Eryi Wang, Mariola Kurowska-Stolarska, Dong Li, Charles McSharry, Damo Xu,Interleukin-33 promoting Th1 lymphocyte differentiation dependents on IL-12, Immunobiology, Volume 221, Issue 3, 2016,Pages 412-417,ISSN 0171-2985,https://doi.org/10.1016/j.imbio.2015.11.013.
76. Nguyen OTP, Misun PM, Lohasz C, Lee J, Wang W, Schroeder T, Hierlemann A. An Immunocompetent Microphysiological System to Simultaneously Investigate Effects of Anti-Tumor Natural Killer Cells on Tumor and Cardiac Microtissues. Front Immunol. 2021 Dec 2;12:781337. doi: 10.3389/fimmu.2021.781337. PMID: 34925361; PMCID: PMC8675866.
77. Ottaviano M, De Placido S, Ascierto PA. Recent success and limitations of immune checkpoint inhibitors for cancer: a lesson from melanoma. Virchows Arch. 2019 Apr;474(4):421-432. doi: 10.1007/s00428-019-02538-4. Epub 2019 Feb 12. PMID: 30747264.
78. Pastille, E., Wasmer, MH., Adamczyk, A. *et al.* The IL-33/ST2 pathway shapes the regulatory T cell phenotype to promote intestinal cancer. *Mucosal Immunol* **12**, 990–1003 (2019). https://doi.org/10.1038/s41385-019-0176-y
79. Patel K, Dickson J, Din S, Macleod K, Jodrell D, Ramsahoye B. Targeting of 5-aza-2'-deoxycytidine residues by chromatin-associated DNMT1 induces proteasomal degradation of the free enzyme. Nucleic Acids Res. 2010 Jul;38(13):4313-24. doi: 10.1093/nar/gkq187. Epub 2010 Mar 25. PMID: 20348135; PMCID: PMC2910061.
80. Qin L, Dominguez D, Chen S, Fan J, Long A, Zhang M, et al. Exogenous IL-33 overcomes T cell tolerance in murine acute myeloid leukemia. Oncotarget. 2016;7(38):61069-80. doi: 10.18632/oncotarget.11179

81. Ralli M, Botticelli A, Visconti IC, Angeletti D, Fiore M, Marchetti P, Lambiase A, de Vincentiis M, Greco A. Immunotherapy in the Treatment of Metastatic Melanoma: Current Knowledge and Future Directions. J Immunol Res. 2020 Jun 28;2020:9235638. doi: 10.1155/2020/9235638. PMID: 32671117; PMCID: PMC7338969.
82. Roussel L, Erard M, Cayrol C, Girard JP. Molecular mimicry between IL-33 and KSHV for attachment to chromatin through the H2A-H2B acidic pocket. EMBO Rep. 2008 Oct;9(10):1006-12. doi: 10.1038/embor.2008.145. Epub 2008 Aug 8. PMID: 18688256; PMCID: PMC2572127.).
83. Russell W. Jenkins, Amir R. Aref, Patrick H. Lizotte, Elena Ivanova, Susanna Stinson, Chensheng W. Zhou, Michaela Bowden, Jiehui Deng, Hongye Liu, Diana Miao, Meng Xiao He, William Walker, Gao Zhang, Tian Tian, Chaoran Cheng, Zhi Wei, Sangeetha Palakurthi, Mark Bittinger, Hans Vitzthum, Jong Wook Kim, Ashley Merlino, Max Quinn, Chandrasekar Venkataramani, Joshua A. Kaplan, Andrew Portell, Prafulla C. Gokhale, Bart Phillips, Alicia Smart, Asaf Rotem, Robert E. Jones, Lauren Keogh, Maria Anguiano, Lance Stapleton, Zhiheng Jia, Michal Barzily-Rokni, Israel Cañadas, Tran C. Thai, Marc R. Hammond, Raven Vlahos, Eric S. Wang, Hua Zhang, Shuai Li, Glenn J. Hanna, Wei Huang, Mai P. Hoang, Adriano Piris, Jean-Pierre Eliane, Anat O. Stemmer-Rachamimov, Lisa Cameron, Mei-Ju Su, Parin Shah, Benjamin Izar, Manisha Thakuria, Nicole R. LeBoeuf, Guilherme Rabinowits, Viswanath Gunda, Sareh Parangi, James M. Cleary, Brian C. Miller, Shunsuke Kitajima, Rohit Thummalapalli, Benchun Miao, Thanh U. Barbie, Vivek Sivathanu, Joshua Wong, William G. Richards, Raphael Bueno, Charles H. Yoon, Juan Miret, Meenhard Herlyn, Levi A. Garraway, Eliezer M. Van Allen, Gordon J. Freeman, Paul T. Kirschmeier, Jochen H. Lorch, Patrick A. Ott, F. Stephen Hodi, Keith T. Flaherty, Roger D. Kamm, Genevieve M. Boland, Kwok-Kin Wong, David Dornan, Cloud Peter Paweletz, David A. Barbie; *Ex Vivo* Profiling of PD-1 Blockade Using Organotypic Tumor Spheroids. *Cancer Discov* 1 February 2018; 8 (2): 196–215. https://doi.org/10.1158/2159-8290.CD-17-0833
84. Russo AE, Torrisi E, Bevelacqua Y, Perrotta R, Libra M, McCubrey JA, Spandidos DA, Stivala F, Malaponte G. Melanoma: molecular pathogenesis and emerging target therapies (Review). Int J Oncol. 2009 Jun;34(6):1481-9. doi: 10.3892/ijo_00000277. PMID: 19424565.
85. Scott, I.C., Majithiya, J.B., Sanden, C. *et al.* Interleukin-33 is activated by allergen- and necrosis-associated proteolytic activities to regulate its alarmin activity during epithelial damage. *Sci Rep* **8**, 3363 (2018). https://doi.org/10.1038/s41598-018-21589-2
86. Shaffer S.M., Dunagin M.C., Torborg S.R., Torre E.A., Emert B., Krepler C., Beqiri M., Sproesser K., Brafford P.A., Xiao M., et al. Rare Cell Variability and Drug-Induced Reprogramming as a Mode of Cancer Drug Resistance. Nature. 2017;546:431–435. doi: 10.1038/nature22794.
87. Shin DY, Kim G, Kim CG, Kim W, Kang HS and Choi YH: Anti-invasive effects of decitabine, a DNA methyltransferase inhibitor, through tightening of tight junctions and inhibition of matrix metalloproteinase activities in AGS human gastric carcinoma cells. Oncol Rep 28: 1043-1050, 2012.
88. Stahl M, Kohrman N, Gore SD, Kim TK, Zeidan AM, et al. (2016) Epigenetics in Cancer: A Hematological Perspective. PLOS Genetics 12(10): e1006193. https://doi.org/10.1371/journal.pgen.1006193
89. Steingrímsson E, Copeland NG, Jenkins NA. Melanocytes and the microphthalmia transcription factor network. Annu Rev Genet. 2004;38:365-411. doi: 10.1146/annurev.genet.38.072902.092717. PMID: 15568981.

90. Sukari A, Abdallah N, Nagasaka M. Unleash the power of the mighty T cells-basis of adoptive cellular therapy. Crit Rev Oncol Hematol. 2019 Apr;136:1-12. doi: 10.1016/j.critrevonc.2019.01.015. Epub 2019 Jan 25. PMID: 30878123.
91. Switzer Benjamin, Puzanov Igor, Skitzki Joseph, J.Hamad Lamya, Ernstoff Marc. Managing Metastatic Melanoma in 2022: A Clinical Review 2022/05/01 JCO Oncology Practice JCO Oncol Pract 335351 18- 5 doi: 10.1200/OP.21.00686 10.1200/OP.21.
92. Tsuda H, Komine M, Karakawa M, Etoh T, Tominaga S-I, Ohtsuki M. Novel splice variants of IL-33: differential expression in normal and transformed cells. *J Invest Dermatol.* (2012) 132:2661–4. doi: 10.1038/jid.2012.180
93. V. Carriere,L. Roussel,N. Ortega,D. Lacorre,L. Americh,L. Aguilar,G. Bouche,& J. Girar d,IL-33, the IL-1-like cytokine ligand for ST2 receptor, is a chromatin-associated nuclear factor *in vivo*, *Proc. Natl. Acad. Sci. U.S.A.* 104 (1) 282 287, https://doi.org/10.1073/pnas.0606854104 (2007).
94. Wagner M, Ealey KN, Tetsu H, Kiniwa T, Motomura Y, Moro K, et al. Tumor-Derived Lactic Acid Contributes to the Paucity of Intratumoral ILC2s. Cell Rep. 2020;30(8):2743-57.e5. doi: 10.1016/j.celrep.2020.01.103.
95. Wen Jie Yeoh, Vivian P. Vu, Philippe Krebs, IL-33 biology in cancer: An update and future perspectives, Cytokine, Volume 157, 2022, 155961, ISSN 1043-4666 https://doi.org/10.1016/j.cyto.2022.155961.
96. x, Tardiveau C, Coudert J, Laffont R, Blanchard L, Bellard E, et al. Tumor associated high endothelial venules mediate lymphocyte entry into tumors and predict response to PD-1 plus CTLA-4 combination immunotherapy. Cancer Cell. 2022;40:318–34.
97. Xia Yulong, Ohno, TatsukuniNishii, Naoto Bhingare, Arundhati Tachinami, Hidetake Kashima, Yoshihisa Nagai, Shigenori Saito, Hirohisa Nakae, Susumu Azuma, Miyuki Endogenous IL-33 exerts CD8+ T cell antitumor responses overcoming pro-tumor effects by regulatory T cells in a colon carcinoma Biochemical and Biophysical Research Communications 518 2 331 336 2019 0006-291X https://doi.org/10.1016/j.bbrc.2019.08.058
98. Xiao P, Wan X, Cui B, Liu Y, Qiu C, Rong J, Zheng M, Song Y, Chen L, He J, Tan Q, Wang X, Shao X, Liu Y, Cao X, Wang Q. Interleukin 33 in tumor microenvironment is crucial for the accumulation and function of myeloid-derived suppressor cells. Oncoimmunology. 2015 Jun 24;5(1):e1063772. doi: 10.1080/2162402X.2015.1063772. PMID: 26942079; PMCID: PMC4760338.
99. Yasuhiro Oki, Etsuko Aoki, Jean-Pierre J. Issa, Decitabine Bedside to bench,Critical Reviews in Oncology/Hematology, Volume 61, Issue 2,2007,Pages 140-152,ISSN 1040-8428,https://doi.org/10.1016/j.critrevonc.2006.07.010.
100. Yeoh WJ, Vu VP, Krebs P. IL-33 biology in cancer: An update and future perspectives. Cytokine. 2022;157:155961. doi: 10.1016/j.cyto.2022.155961.
101. Yeon-Sook Choi, Hyun-Jung Choi, Jeong-Ki Min, Bo-Jeong Pyun, Yong-Sun Maeng, Hongryeol Park, Jihye Kim, Young-Myeong Kim, Young-Guen Kwon; Interleukin-33 induces angiogenesis and vascular permeability through ST2/TRAF6-mediated endothelial nitric oxide production. *Blood* 2009; 114 (14): 3117–3126. doi: https://doi.org/10.1182/blood-2009-02-203372
102. Yi S.-J., Hwang S.Y., Oh M.-J., Kim Y.-H., Ryu H., Rhee S.-K., Jhun B.H., Kim K. Oncogenic N-Ras Stimulates SRF-Mediated Transactivation via H3 Acetylation at Lysine 9. BioMed Res. Int. 2018;2018:5473725. doi: 10.1155/2018/5473725.
103. Yu G, Wu Y, Wang W, Xu J, Lv X, Cao X, et al. Low-dose decitabine enhances the effect of PD-1 blockade in colorectal cancer with microsatellite stability by re-modulating the tumor microenvironment. Cell Mol Immunol. 2019;16(4):401-9. doi: 10.1038/s41423-018-0026-y.

104. Yue J, Guo H, Xu P, Ma J, Shi W, Wu Y. Combination of IL-33 with PD-1 blockade augment mILC2s-mediated anti-tumor immunity. Cancer Immunol Immunother. 2024;73(4):65. doi: 10.1007/s00262-023-03580-7.
105. Zhang F, Tossberg JT, Spurlock CF, Yao SY, Aune TM, Sriram S. Expression of IL-33 and its epigenetic regulation in Multiple Sclerosis. Ann Clin Transl Neurol. 2014;1(5):307-18. doi: 10.1002/acn3.47.
106. Zhang P, Tao C, Lu Y, Li P, Wang X, Dai Y, Xi Y, Shimura T, Li X, Fang J, Yang L, He D, Guo P. Epigenetic Reprogramming Potentiates ICAM1 Antibody Drug Conjugates in Preclinical Models of Melanoma. Adv Sci (Weinh). 2024 Aug;11(30):e2400203. doi: 10.1002/advs.202400203. Epub 2024 Jun 14. PMID: 38874532; PMCID: PMC11321650.
107. Zhang, Tian Tian, Chaoran Cheng, Zhi Wei, Sangeetha Palakurthi, Mark Bittinger, Hans Vitzthum, Jong Wook Kim, Ashley Merlino, Max Quinn, Chandrasekar Venkataramani, Joshua A. Kaplan, Andrew Portell, Prafulla C. Gokhale, Bart Phillips, Alicia Smart, Asaf Rotem, Robert E. Jones, Lauren Keogh, Maria Anguiano, Lance Stapleton, Zhiheng Jia, Michal Barzily-Rokni, Israel Cañadas, Tran C. Thai, Marc R. Hammond, Raven Vlahos, Eric S. Wang, Hua Zhang, Shuai Li, Glenn J. Hanna, Wei Huang, Mai P. Hoang, Adriano Piris, Jean-Pierre Eliane, Anat O. Stemmer-Rachamimov, Lisa Cameron, Mei-Ju Su, Parin Shah, Benjamin Izar, Manisha Thakuria, Nicole R. LeBoeuf, Guilherme Rabinowits, Viswanath Gunda, Sareh Parangi, James M. Cleary, Brian C. Miller, Shunsuke Kitajima, Rohit Thummalapalli, Benchun Miao, Thanh U. Barbie, Vivek Sivathanu, Joshua Wong, William G. Richards, Raphael Bueno, Charles H. Yoon, Juan Miret, Meenhard Herlyn, Levi A. Garraway, EliezerM. Van Allen, Gordon J. Freeman, Paul T. Kirschmeier, Jochen H. Lorch, Patrick A. Ott, F. Stephen Hodi, Keith T. Flaherty, Roger D. Kamm, Genevieve M. Boland, Kwok-Kin Wong, David Dornan, Cloud Peter Paweletz, David A. Barbie; *Ex Vivo* Profiling of PD-1 Blockade Using Organotypic Tumor Spheroids. *Cancer Discov* 1 February 2018; 8 (2): 196–215. https://doi.org/10.1158/2159-8290.CD-17-0833